

UC San Diego

UC San Diego Electronic Theses and Dissertations

Title

Structural and functional characterization of the p53 C- terminus

Permalink

<https://escholarship.org/uc/item/6w05v3wb>

Author

Kim, Sun Kyung

Publication Date

2012

Peer reviewed|Thesis/dissertation

UNIVERSITY OF CALIFORNIA, SAN DIEGO

Structural and Functional Characterization of the p53 C-terminus

A Thesis submitted in partial satisfaction of the requirements for the degree
Master of Science

in

Chemistry

by

Sun Kyung Kim

Committee in charge:

Professor Hector Viadiu, Chair
Professor Ulrich Muller
Professor Douglas Magde

2012

Copyright
Sun Kyung Kim, 2012
All rights reserved.

The Thesis of Sun Kyung Kim is approved and it is acceptable in quality and form for publication on microfilm and electronically:

Chair

University of California, San Diego

2012

DEDICATION

I would first like to dedicate this Master's thesis to Jesus, my Savior and my Redeemer. I would also like to dedicate this thesis to my parents who loved me unconditionally all my life, and without their love this thesis would not have been possible.

TABLE OF CONTENTS

Signature Page.....	iii
Dedication.....	iv
Table of Contents.....	v
List of Figures.....	vii
List of Tables.....	ix
Acknowledgements.....	x
Abstract of the Thesis.....	xii
Chapter One.....	1
Introduction	
Regulation of p53.....	2
Domains of p53.....	4
Current knowledge on p53 Regulatory domain.....	6
Objective of the Thesis.....	7
References.....	15
Chapter Two.....	18
Structural Study of the p53 C-terminus	
Introduction.....	19
Materials and Methods.....	21
Results.....	26
Discussion.....	28
References.....	41
Chapter Three.....	43
Functional Characterization of the p53 C-terminus: p53CT DNA Binding	

Introduction.....	44
Materials and Methods.....	46
Results.....	48
Discussion.....	49
References.....	54
Chapter Four.....	56
Functional Characterization of the p53 C-terminus: Regulation by MDM2	
Introduction.....	57
Materials and Methods.....	59
Results.....	64
Discussion.....	68
References.....	82

LIST OF FIGURES

Figure 1.1a,b Regulation of p53 in normal cells.....	10
Figure 1.2 Regulation of p53 and MDM2 under cellular stress.....	11
Figure 1.3 Domains of the p53 protein	12
Figure 1.4 Structure of the DBD and the TD of p53.....	13
Figure 1.5 Breakdown of Thesis By Chapters	14
Figure 2.1a Dimer of p53CT Tetramerization Domain	29
Figure 2.1b Tetramer of p53CT Tetramerization Domain	29
Figure 2.2 p53CT construct	30
Figure 2.3 15% SDS-PAGE of p53CT expression and purification.....	31
Figure 2.4 Mono S chromatography separating MBP (pI 5.05) from p53CT (pI 8.35)	32
Figure 2.5 Desalt Chromatogram of pure p53CT concentrated and run on Sephadex 25	33
Figure 2.6 MALDI-TOF spectrum of p53CT wildtype protein.....	34
Figure 2.7 MALDI-TOF spectrum of Se-MET incorporated p53CT protein.....	35
Figure 2.8 Se-MET incorporated p53CT protein crystals.....	36
Figure 2.9 X-ray diffraction pattern of Se-MET incorporated p53CT.....	37
Figure 2.10a Electron density of Se-MET observed by the MAD method.....	38
Figure 2.10b Building of the p53CT structure starting from the Se-MET site.....	38
Figure 2.11 Unit cell packing of p53CT crystal	39
Figure 3.1 DNA length vs. Sedimentation coefficient.....	51
Figure 4.1 Domains of MDM2.....	71

Figure 4.2 SDS-PAGE of 6xHis MDM2 Purification	72
Figure 4.3 Western Blot of 6xHis MDM2 Purification	72
Figure 4.4 Gel filtration chromatogram of wild type MDM2	73
Figure 4.5 10% SDS-PAGE of wild type MDM2 preparation with 0.1 mM zinc chloride	74
Figure 4.6 Western blot of wild type MDM2 preparation with 0.1mM zinc chloride, blotted with anti-his antibody	74
Figure 4.7 Preparation of MDM2 Δ C7 resolved in 10% SDS-PAGE.....	75
Figure 4.8 Truncated MDM2 Δ C7 mutant with 0.1 mM zinc chloride.....	75
Figure 4.9 Gel filtration profile of the truncated mutant MDM2 Δ C7	76
Figure 4.10 Truncated mutant resolved in 7% SDS-PAGE and visualized by Coomassie staining	77
Figure 4.11 Western blots of MDM2-MBP Preparation.....	78
Figure 4.12 Gel filtration profile of MDM2-MBP	79
Figure 4.13 Fractions of MDM2-MBP gel filtration profile concentrated and resolved in 10% SDS-PAGE	79
Figure 4.14 Electron micrographs of MDM2-MBP	80
Figure 4.15 Electron micrographs of wild type MDM2	80
Figure 4.16 Co-expression experiment of MDM2 and p53CT.....	81

LIST OF TABLES

Table 2.1 Refinement table of p53CT structure	40
Table 3.1 Sedimentation Coefficients of Various DNAs.....	51
Table 3.2 Summary of sedimentation velocity experiments with specific and non-specific DNAs	52
Table 3.3 Specific DNA sequences	52
Table 3.4 Non-specific DNA sequences	53

ACKNOWLEDGEMENTS

I would first like to thank my family for their support throughout my time as a master's student. Without their unconditional love and support in every way, I would not have had a chance to pursue my master's study and be able to come this far as a student. Especially, I would like to thank my Mom and Dad for believing in me and supporting my dream as a scientist. And I also thank my grandparents for their love and encouragements. And I thank my grandparents and aunt for their financial support as well to help pay for my education.

I would like to thank my graduate advisor, Dr. Viadiu for his time and effort in making this thesis dissertation possible. Without his diligence and care in coaching me throughout my preparation for this dissertation, this dissertation would not have been possible. I thank him for being my guide for the past two and a half years I spent in his lab. In addition, I thank Dr. Magde and Dr. Muller for serving on my committee and providing helpful feedbacks on this thesis.

I also thank the members of my lab. First, I thank Eleanor Sano for diligently helping me in protein purification in the days approaching my thesis defense. Her help and care enabled me to complete the dissertation on time. I also thank Dr. Ethayathulla Abdul for carrying out all the data collection and processing for the crystallography project. And I thank him for spending time teaching me in techniques and knowledge that I lacked. I also thank Ana Ramos for being my support throughout the years. She became a role model for me

exemplifying her hard work and joy in doing science. Her courage and persistence are sources of inspiration for me. I thank Ha Nguyen for aiding me in protein purification and in helping me in formatting my thesis, and giving me helpful advice and encouragements. I also want to thank Thien Nguyen and Kevin Lefever for proofreading my thesis and critiquing my dissertation talk. I thank Frank for sharing his advice on protein purification and also sharing his stock of PreScission protease.

I also want to thank Nikki Cheung for inviting me to this lab and allowing me to explore scientific research. She is also a mentor and a friend with whom I can share the joy and the sorrows of life and be comforted and encouraged. She has been a great source of support not only in science but also in making me into the person I am today. I am forever grateful for her love and support. I also thank previous member Aki Tse for her help in teaching me basic techniques in lab and also in analyzing AUC data. I also thank Dr. Akama for coaching me in improving the basic techniques in the lab.

Lastly, I want to thank my boyfriend Philip Kay for his love and support throughout my master's program. Without his patience and love for me, I would not be where I am today. I also want to thank Nari Kwon for her love and nurturing for the past three years. Our friendship has encouraged and supported me throughout the challenging days.

ABSTRACT OF THE THESIS

Structural and Functional Characterization of the p53 C-terminus

by

Sun Kyung Kim

Master of Science in Chemistry

University of California, San Diego, 2012

Professor Hector Viadiu, Chair

The p53 tumor suppressor protein is an important molecule studied extensively in cancer research. In order to study the mechanism of tumor suppression by p53, structural knowledge is needed. Although the structure of the p53 DNA binding domain bound to DNA has been well elucidated, there is a lack of structural knowledge of the regulatory domain of p53 bound to the DNA.

Structural knowledge of this domain bound to the DNA would contribute to the full understanding of the p53 tumor suppression mechanism. In order to solve this problem, X-ray crystallography was used to elucidate the p53 regulatory domain structure. In order to facilitate the crystallization of p53 regulatory domain with DNA, oligomerization of p53 with various DNAs was studied using the sedimentation velocity method. Functional aspects of p53 regulation were studied including acetylation and interaction with the MDM2 protein. It has been found that the p53 regulatory domain binds to both the consensus and non-consensus DNA as a tetramer, and the interaction of the p53 regulatory domain with MDM2 produces a novel MDM2 oligomerization state.

Chapter One

Introduction

1.1 Regulation of p53

p53 is a nucleoprotein that functions as a transcription factor. It is often called “the guardian of the genome” because it activates cellular pathways against tumor progression (Teodoro *et al.*). Inactivation of the p53 protein through deletion, mutation or interaction with other cellular or viral proteins is observed in over 50% of human cancers (Ayed *et al.*). The prevalence of mutant p53 in cancer cases underlines the importance of p53’s role as a tumor suppressor. Most of these mutations are found in the DNA binding domain of p53 and disrupt its activity as a transcription factor (Levine *et al.*).

In normal cells, when the p53 tumor suppression activity is not needed, p53 levels are kept low by a negative regulator protein known as Murine Double Minute 2 (MDM2) (Levine *et al.*). MDM2 triggers p53 proteasomal degradation by attaching ubiquitin molecules to lysine residues in the C-terminus of p53 (Figure 1.1a) (Cheng *et al.*, 2009). The dimerization of the MDM2 C-terminal RING domain is required for the MDM2 scaffold formation and for the elongation of the ubiquitin chain. It has been postulated that the higher order RING-domain oligomers aid in the formation of ubiquitin chains and, thus, p53 is degraded in the cells when an elongated ubiquitin chain gets transferred to the C-terminal lysine residues of p53.

Upon cellular stress, such as DNA damage and hypoxia, the cellular levels of p53 are increased by the inhibition of MDM2 ubiquitinating activity (Cheng *et al.*, 2010) (Figure 1.1b). The inhibition of MDM2 activity is achieved by the ATM kinase, which phosphorylates the residues near the RING domain of MDM2

inhibiting the MDM2 oligomerization needed for p53 ubiquitination (Cheng *et al.*, 2009). In addition to the ATM kinase, MDM2 is also phosphorylated by ATR and c-Abl, but this phosphorylation does not inhibit the MDM2 E3 ligase activity and the phosphorylated MDM2 can still mono-ubiquitinate p53 (Cheng *et al.*, 2010). However, monomeric RING domains cannot synthesize the poly-ubiquitin chains required for the proteasomal degradation of p53 (Cheng *et al.*, 2010) (Figure 1.2).

It has been shown that p53 is also phosphorylated in the N-terminal transactivation domain (TAD) by kinases such as Chk2, DNA PK and ATM (Cheng *et al.*, 2010) (Figure 1.2). The N-terminus phosphorylation inhibits p53 interaction with MDM2, enabling the recruitment of additional transcriptional cofactors and the rest of the transcriptional machinery (Cheng *et al.*, 2010).

An additional regulatory mechanism of the cellular p53 levels upon DNA damage involves an auto-inhibitory loop where p53 activates the transcription of the gene of its negative regulator MDM2. This regulatory feedback loop further regulates the amount of active p53 in the cell, by increasing the expression of MDM2 when the cellular concentration of p53 increases (Figure 1.2) (Levine *et al.*).

Active p53 binds upstream of the transcription start site of its target genes and increases its rate of transcription by recruiting other transcription factors and the mediator complex to the promoter site (Levine *et al.*). Upon the accumulation of p53 in the nucleus, depending on the severity of the cellular damage, over 100 downstream transcriptional targets are expressed to suppress tumor formation

that either inhibit cell cycle progression or promote apoptosis (Cheng *et al.*, 2010). First, during cell cycle arrest, p53 activates the expression of genes such as *WAF1* which expresses the p21 protein. p21 binds to the G1-S/CDK and S/CDK complexes halting the progression into the S-phase of the cell cycle (Levine *et al.*). Meanwhile, DNA repair proteins fix the damaged DNA before the cell cycle can resume. Second, during the apoptotic pathway, p53 activates the expression of proapoptotic genes of the Bcl-2 protein family, such as PUMA and Noxa that ultimately lead to cell death (Levine *et al.*).

1.2 Domains of p53

p53 belongs to a family of proteins which includes two more ancient members, p63 and p73, that are predominately involved in development. All share a basic gene structure (Ou *et al.*). The p53 gene codifies for a 393 amino acid protein made of multiple domains that contribute to its function as a transcription factor (Figure 1.3).

The N-terminal transactivation domain (TAD) is composed of two parts where TAD1 (aa 1-42) activates transcription factors and TAD2 (aa 43-63) is important for the apoptotic activity (Lane *et al.*). The TAD mediates interaction with coactivators and also with the regulatory protein MDM2. Binding of MDM2 to the N-terminus of p53 inhibits p53 transcriptional activity.

The proline-rich domain is composed of amino acids 64-97 and is important for the apoptotic activity of p53 (Lane *et al.*).

The central domain of p53 is the DNA-binding domain (aa 98-300) that enables coactivator recruitment by the TAD because the DBD has a nanomolar affinity for the consensus (specific) DNA sequences found in the response elements of the p53 target genes (Levine *et al.*). This region is the most commonly mutated region of the protein and mutations are observed in over 50% of human cancer cells (Levine *et al.*).

The nuclear localization signaling domain (aa 316-325) allows the transport of the protein between the nucleus and the cytosol (Lane *et al.*).

The tetramerization domain (aa 324-355) provides contact residues for the oligomerization of the protein to form homo-tetramer assembly as a dimer of dimers (Lane *et al.*) (Figure 1.4). The formation of tetramers is important for the activity of p53 *in vivo* and crystal structures show that p53 binds DNA as a tetramer (Malecka *et al.*) (Figure 1.4). In solution, the tetramer seems to be the functional unit, although dimers can also be observed at lower protein concentrations (Weinberg, Veprintsev *et al.*).

The C-terminal regulatory domain (aa 360-393) is intrinsically disordered and adopts an α -helical or a β -hairpin structures upon binding to other proteins (Ayed *et al.*). It binds non-specifically to DNA with a micromolar affinity and it has been found to negatively regulate the DNA binding activity of the DNA-binding domain.

1.3 Current knowledge on the p53 Regulatory Domain

NMR spectroscopy has shown that the regulatory domain (RD) of p53 (aa 360-393) has no regular structure in its native form (Ayed *et al.*). To date, there is no crystal structure of this region alone, as this unstructured region is very dynamic and therefore difficult to crystallize. As mentioned before, binding to other proteins induces conformation in this region. In 2000, the NMR structure of the regulatory domain bound to S100B($\beta\beta$) was solved (Rustandi *et al.*). When bound to this calcium binding protein, the RD exhibited a helical conformation. It is an important goal of p53 research to obtain a structure of the RD bound to DNA, as this interaction is important in the overall transactivation mechanism. It has been speculated that a weaker binding of the RD to DNA allows the protein to “scan” the DNA molecule until it reaches the target gene response element where the DBD then binds with a stronger affinity.

The role of the p53 RD has not been clearly elucidated and there are controversies regarding its role in regulation of the DNA binding activity of the DBD. The regulatory domain of p53 is known to inhibit DBD's specific binding (Weinberg, Freund *et al.*). There have been two proposed models for this inhibition (Ayed *et al.*). The first model is an allosteric mechanism where the RD interaction with other domains of p53 leads to the inhibition of the DNA binding by the DBD. The second model is a competitive mechanism where both domains, the RD and the DBD, compete for DNA binding. NMR studies have disproved the allosteric model by showing that constructs with and without RD have the identical conformation and that RD does not interact with any other

domains (Ayed *et al.*). The competitive model is supported by recent data where the specific DNA binding by the DBD is abolished in the presence of an excess of non-specific DNA where the RD would be expected to be bound to the non-specific DNAs (Weinberg, Freund *et al.*). p53 is said to be in a “latent” DNA binding state when the RD has no post-translational modifications. Weinberg study shows that the presence of the RD *per se* does not inhibit the specific DNA binding activity of the DBD, but rather the non-specific DNA binding to RD inhibits the specific DNA binding through the DBD. However, how the non-specific DNA binding by the RD occurs is not yet known and no structure has yet been determined to understand the non-specific DNA binding.

1.4 Objectives of the Thesis

There is an extensive body of research being conducted around the world on the p53 tumor suppressor protein. The National Library of Medicine shows that over 60,000 scientific papers have been published on this molecule since its discovery in 1979. Because of its importance in cancer, scientists are trying to find new ways to tap p53 and its related pathways to discover novel cancer therapies.

The aim of my thesis was to obtain a crystal structure of p53CT (Tetramerization Domain + Regulatory Domain) either alone or in the presence of DNA. We tested the various DNAs that have been successfully used to crystallize with the DNA binding domain as suitable candidates for crystallizing with the regulatory domain.

In order to help optimize the crystallization of p53CT with DNA, sedimentation velocity experiments were conducted with a panel of specific and non-specific DNA molecules of varied lengths. An increase in the sedimentation coefficient gives clues to which DNA binds to the protein and the percentage of each peak shows measures of its affinity binding. In this study, we also created a dimer mutant of p53CT (M340Q, L344R). If this dimer mutant crystallizes with DNA, the structure will confer true symmetry to the tetramerization domain that is still controversial.

Acetylation is a post-translational modification common in cell signaling. Its functional role in p53 has been related to an increase in the DNA binding affinity by the DBD (Arbely *et al.*). Acetylation was also hypothesized to have a role in co-activator recruitment and cellular localization (Prives *et al.*). We created acetylated mutants of p53CT to study their effect on DNA binding by the regulatory domain.

Lastly, we studied the functional aspect of the p53CT. To understand p53 regulation, it is important to know how p53 is negatively regulated by the interaction with MDM2. It has been reported that the C-terminus of p53 not only interacts with the MDM2 RING domain, but it also binds to the MDM2 N-terminus (Poyurovsky *et al.*, 2010). In this thesis, I studied the oligomerization states of various mutants of MDM2 and the effect of p53CT on MDM2 oligomerization. As a summary of my thesis encompassing the structural and functional studies of

the p53 C-terminus, Figure 1.5 illustrates the various aspects of the characterization of the p53 C-terminus studied in this thesis.

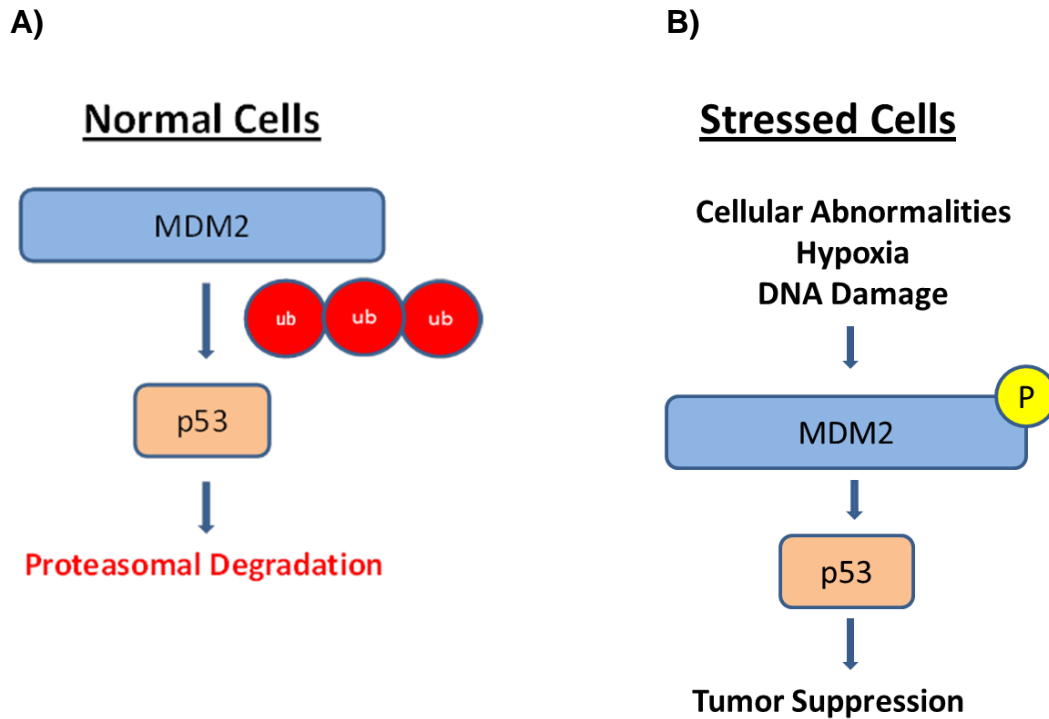


Figure 1.1a,b Regulation of p53 in normal cells. During homeostasis in normal cells, MDM2 ubiquitinates p53 for proteasomal degradation. Upon cellular stress, phosphorylation on MDM2 inhibits ubiquitination of p53.

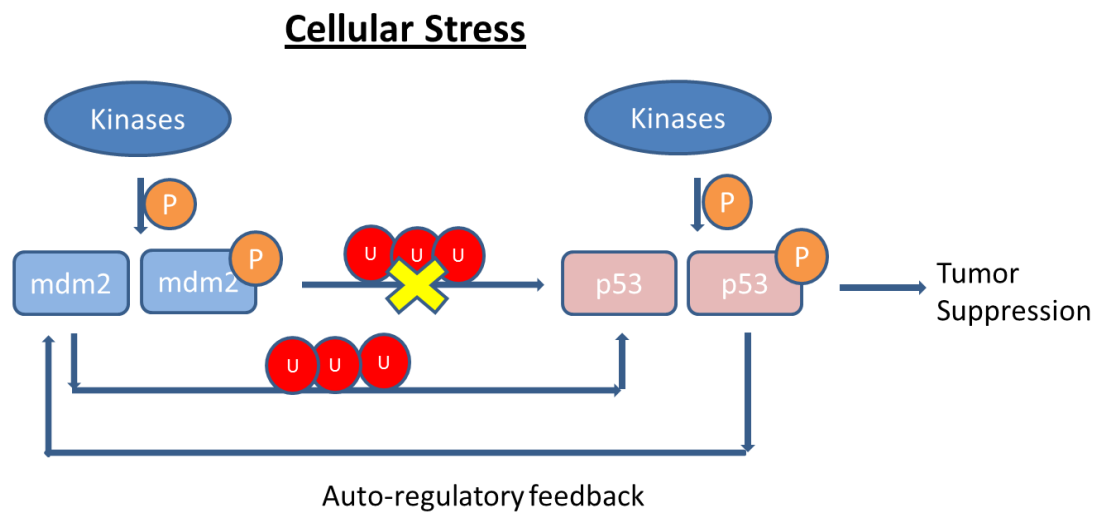


Figure 1.2 Regulation of p53 and MDM2 under cellular stress. Upon cellular stress such as DNA damage, kinases phosphorylate MDM2. Phosphorylated MDM2 cannot poly-ubiquitinate p53, and p53 is free from inhibition by MDM2. A separate set of kinases phosphorylate p53, and this inhibits physical interaction with MDM2. Free p53 is active in tumor suppression. In auto-regulatory feedback regulation, p53 can activate MDM2 transcription, which in turn regulates p53 levels in the cell.



Figure 1.3 Domains of the p53 protein. p53 protein is composed of five distinct regions. Transactivation domain (TAD) is involved in transcription activation by interacting with coactivators and the transcription machinery. Proline rich region (PRR) is involved in the apoptotic activity of p53. DNA binding domain (DBD) is the most mutated region that leads to over 50% of human cancers. It binds specific DNA with nanomolar affinity. Tetramerization domain (TD) forms homotetramers as dimer of dimers that allows appropriate contacts in DNA binding. Regulatory domain (RD) is an unstructured region that adopts structure upon ligand binding. It binds DNA non-specifically with micromolar affinity.

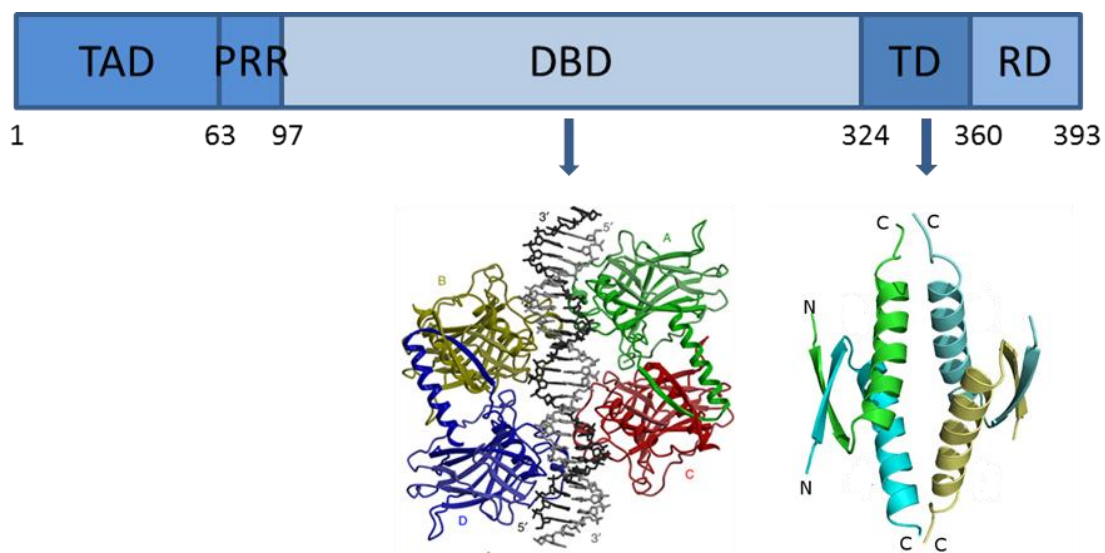


Figure 1.4 Structure of the DBD and the TD of p53. Crystal structures showing the DNA binding domain of p53 bound to the DNA as a tetramer (dimer of dimers), and the crystal structure of the packing of the tetramerization domain of p53 with different colored peptides denoting each monomer.

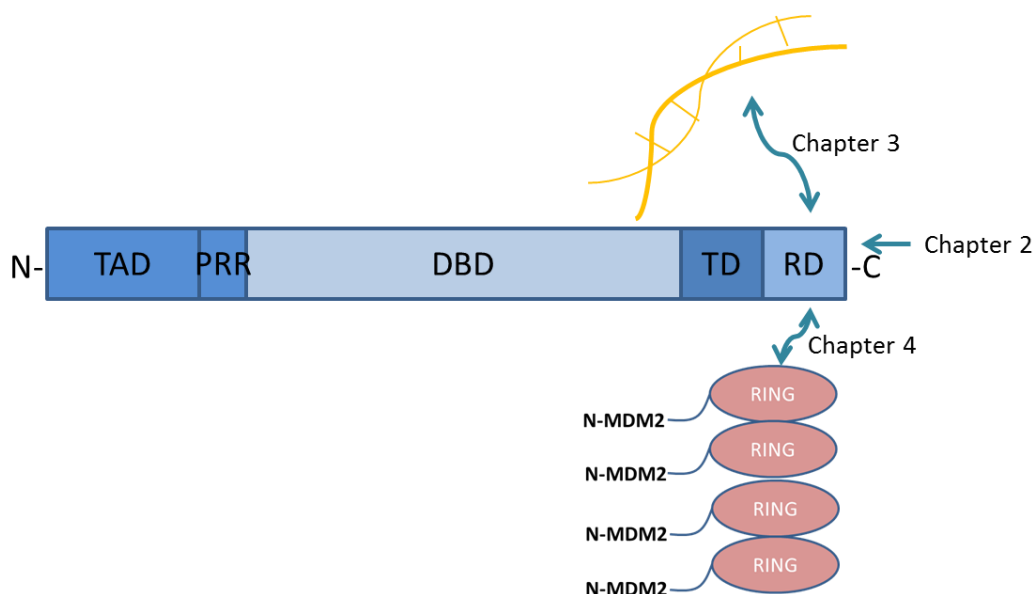


Figure 1.5 Breakdown of Thesis By Chapters. In Chapter 2, I studied the structure of p53CT including the tetramerization (TD) and the regulatory domains (RD) using X-ray crystallography. In Chapter 3, I studied the DNA binding of p53CT using sedimentation velocity method with analytical ultracentrifugation. I also explored the p53CT dimerization mutant and acetylation mutants for future DNA binding studies. In Chapter 4, I studied the interaction of p53CT with MDM2, which is the principal negative inhibitor of p53.

References

- Arbely, E.; Natan, E.; Brandt, T.; Allen, M. D.; Veprintsev, D. B.; Robinson, C. V.; Chin, J. W.; Joerger, A. C.; Fersht, A. R., Acetylation of lysine 120 of p53 endows DNA-binding specificity at effective physiological salt concentration. *Proceedings of the National Academy of Sciences of the United States of America* 2011, 108 (20), 8251-6.
- Ayed, A.; Mulder, F. A.; Yi, G. S.; Lu, Y.; Kay, L. E.; Arrowsmith, C. H., Latent and active p53 are identical in conformation. *Nature structural biology* 2001, 8 (9), 756-60.
- Chen, Y.; Dey, R.; Chen, L., Crystal structure of the p53 core domain bound to a full consensus site as a self-assembled tetramer. *Structure* 2010, 18 (2), 246-56.
- Chen, C.; Gorlatova, N.; Kelman, Z.; Herzberg, O., Structures of p63 DNA binding domain in complexes with half-site and with spacer-containing full response elements. *Proceedings of the National Academy of Sciences of the United States of America* 2011, 108 (16), 6456-61.
- Cheng, Q.; Chen, J., Mechanism of p53 stabilization by ATM after DNA damage. *Cell Cycle* 2010, 9 (3), 472-8.
- Cheng, Q.; Chen, L.; Li, Z.; Lane, W. S.; Chen, J., ATM activates p53 by regulating MDM2 oligomerization and E3 processivity. *The EMBO journal* 2009, 28 (24), 3857-67.
- Cho, Y.; Gorina, S.; Jeffrey, P. D.; Pavletich, N. P., Crystal structure of a p53 tumor suppressor-DNA complex: understanding tumorigenic mutations. *Science* 1994, 265 (5170), 346-55.
- Emamzadah, S.; Tropia, L.; Halazonetis, T. D., Crystal structure of a multidomain human p53 tetramer bound to the natural CDKN1A (p21) p53-response element. *Molecular cancer research : MCR* 2011, 9 (11), 1493-9.
- Ho, W. C.; Fitzgerald, M. X.; Marmorstein, R., Structure of the p53 core domain dimer bound to DNA. *The Journal of biological chemistry* 2006, 281 (29), 20494-502.
- Itahana, K.; Mao, H.; Jin, A.; Itahana, Y.; Clegg, H. V.; Lindstrom, M. S.; Bhat, K. P.; Godfrey, V. L.; Evan, G. I.; Zhang, Y., Targeted inactivation of Mdm2 RING finger E3 ubiquitin ligase activity in the mouse reveals mechanistic insights into p53 regulation. *Cancer cell* 2007, 12 (4), 355-66.

Joerger, A. C.; Rajagopalan, S.; Natan, E.; Veprintsev, D. B.; Robinson, C. V.; Fersht, A. R., Structural evolution of p53, p63, and p73: implication for heterotetramer formation. *Proceedings of the National Academy of Sciences of the United States of America* **2009**, *106* (42), 17705-10.

Kaesler, M. D.; Iggo, R. D., Chromatin immunoprecipitation analysis fails to support the latency model for regulation of p53 DNA binding activity in vivo. *Proceedings of the National Academy of Sciences of the United States of America* **2002**, *99* (1), 95-100.

Kim, H.; Kim, K.; Choi, J.; Heo, K.; Baek, H. J.; Roeder, R. G.; An, W., p53 requires an intact C-terminal domain for DNA binding and transactivation. *Journal of molecular biology* **2012**, *415* (5), 843-54.

Kitayner, M.; Rozenberg, H.; Kessler, N.; Rabinovich, D.; Shaulov, L.; Haran, T. E.; Shakked, Z., Structural basis of DNA recognition by p53 tetramers. *Molecular cell* **2006**, *22* (6), 741-53.

Kitayner, M.; Rozenberg, H.; Rohs, R.; Suad, O.; Rabinovich, D.; Honig, B.; Shakked, Z., Diversity in DNA recognition by p53 revealed by crystal structures with Hoogsteen base pairs. *Nature structural & molecular biology* **2010**, *17* (4), 423-9.

Lane, D. P.; Cheek, C. F.; Brown, C.; Madhumalar, A.; Ghadessy, F. J.; Verma, C., Mdm2 and p53 are highly conserved from placozoans to man. *Cell Cycle* **2010**, *9* (3), 540-7.

Levine, A. J., p53, the cellular gatekeeper for growth and division. *Cell* **1997**, *88* (3), 323-31.

Malecka, K. A.; Ho, W. C.; Marmorstein, R., Crystal structure of a p53 core tetramer bound to DNA. *Oncogene* **2009**, *28* (3), 325-33.

Ou, H. D.; Lohr, F.; Vogel, V.; Mantele, W.; Dotsch, V., Structural evolution of C-terminal domains in the p53 family. *The EMBO journal* **2007**, *26* (14), 3463-73.

Petty, T. J.; Emamzadah, S.; Costantino, L.; Petkova, I.; Stavridi, E. S.; Saven, J. G.; Vauthey, E.; Halazonetis, T. D., An induced fit mechanism regulates p53 DNA binding kinetics to confer sequence specificity. *The EMBO journal* **2011**, *30* (11), 2167-76.

Poyurovsky, M. V.; Priest, C.; Kentsis, A.; Borden, K. L.; Pan, Z. Q.; Pavletich, N.; Prives, C., The Mdm2 RING domain C-terminus is required for

supramolecular assembly and ubiquitin ligase activity. *The EMBO journal* **2007**, 26 (1), 90-101.

Poyurovsky, M. V.; Katz, C.; Laptenko, O.; Beckerman, R.; Lokshin, M.; Ahn, J.; Byeon, I. J.; Gabizon, R.; Mattia, M.; Zupnick, A.; Brown, L. M.; Friedler, A.; Prives, C., The C terminus of p53 binds the N-terminal domain of MDM2. *Nature structural & molecular biology* **2010**, 17 (8), 982-9.

Prives, C.; Manley, J. L., Why is p53 acetylated? *Cell* **2001**, 107 (7), 815-8.

Rustandi, R. R.; Baldisseri, D. M.; Weber, D. J., Structure of the negative regulatory domain of p53 bound to S100B(beta-beta). *Nature structural biology* **2000**, 7 (7), 570-4.

Teodoro, J. G.; Evans, S. K.; Green, M. R., Inhibition of tumor angiogenesis by p53: a new role for the guardian of the genome. *J Mol Med (Berl)* **2007**, 85 (11), 1175-86.

Weinberg, R. L.; Freund, S. M.; Veprintsev, D. B.; Bycroft, M.; Fersht, A. R., Regulation of DNA binding of p53 by its C-terminal domain. *Journal of molecular biology* **2004**, 342 (3), 801-11.

Weinberg, R. L.; Veprintsev, D. B.; Fersht, A. R., Cooperative binding of tetrameric p53 to DNA. *Journal of molecular biology* **2004**, 341 (5), 1145-59.

Yu, J.; Zhang, L., The transcriptional targets of p53 in apoptosis control. *Biochemical and biophysical research communications* **2005**, 331 (3), 851-8.

Chapter Two

Structural Study of the p53 C-terminus

Introduction

p53 is a tumor suppressor protein that becomes activated upon cellular stress, such as DNA damaging agents, inhibitors of RNA synthesis or other cellular stressors (heat shock or hypoxia) (Levine *et al.*). Its role is to activate the transcription of genes that are involved in DNA repair, cell cycle arrest or apoptosis to halt tumor progression (Ayed *et al.*). As a transactivator, p53 binds to the DNA upstream of the promoter site with nanomolar affinity through the DNA binding domain (Ayed *et al.*). Crystal structures have elucidated how this domain binds to DNA (Cho *et al.*, Chen *et al.*, 2010). A tetramer of p53 binds DNA specifically to a response element formed by two decameric half-sites with a PuPuPuC(A/T)(A/T)GPyPyPy (Pu=Purine, Py=Pyrimidine) consensus sequence. Both half-sites can be separated by up to 14 base pairs with most of the functional sites separated by 3 nucleotides (Riley *et al.*). Each p53 monomer binds to one 5 bp PuPuPuC(A/T) quarter site.

Another domain of the transcription factor p53, the C-terminal regulatory domain, has the ability to bind DNA non-specifically. However, the structure of the regulatory domain (amino acids 360 to 393) is not yet known. This region binds DNA non-specifically with micromolar affinity (Kaeser *et al.*). It is initially disordered, and it adopts different secondary structures upon binding to regulatory proteins (Weinberg, Freund *et al.*). Because the C-terminal regulatory domain of p53 regulates the DNA binding of the central DBD, to understand how p53 regulatory domain binds to DNA is critical in understanding the regulation of p53 function. In this thesis I aimed to solve the structure of a construct of p53 C-

terminal domain (p53CT) containing residues 323 to 393 by X-ray crystallography.

The protein construct with amino acids 323 to 393 contains the tetramerization domain (323-355) and the regulatory domain (356-393) of p53. The crystal structure of the tetramerization domain has already been solved in our lab and also in other labs, and each monomer has an alpha-helix and a beta-strand that interacts with another monomer to form a dimer (Figure 2.1a). This dimer comes together with another dimer through the hydrophobic core of the alpha helices to form a tetramer (Figure 2.1b).

However, it has not yet been possible to solve the crystal structure of the regulatory domain due to the difficulties of crystallizing a region with intrinsic flexibility that can only adopt secondary structures upon ligand binding. An NMR structure of p53 amino acids 367 to 388 in complex with the calcium binding protein S100B($\beta\beta$), shows that amino acids 367 to 388 adopt a helical structure (Rustandi *et al.*).

The initial goal of my thesis was to elucidate the structure of p53CT in complex with DNA using X-ray crystallography. I continued the previous crystallization work carried out by Nikki Cheung, a former graduate student in the laboratory (Cheung, 2010). In order to solve the structure, we utilized the Multiple Anomalous Diffraction (MAD) method. Selenomethione containing p53CT proteins were used to grow the crystals. Incorporation of heavy atoms such as Zn, Se, and Hg is commonly used in SAD (Single-) or MAD methods, and it helps

to solve the phase problem where molecular replacement method cannot be used.

Materials and Methods

Construct

The p53CT construct consists of the maltose binding protein (MBP) fused to the tetramerization and regulatory domains of p53 inserted into the pMAL expression vector (Figure 2.2). A linker region with a sequence that can be cleaved by the PreScission protease was inserted between the MBP tag and the p53CT protein (Figure 2.2). The PreScission protease cleaves between the Gln and Gly residues within the recognition sequence LeuGluValLeuPheGln/GlyPro. The pMAL expression vector containing the described protein construct and the ampicillin resistant gene was used to transform the *E. coli* BL21 (DE3) cells.

Expression

The wild type p53CT protein was expressed after an initial overnight culture of *E. coli* BL21 cells grown in 5ml of Luria-Bertoni media (LB). 100 µg/ml of ampicillin was added to 1L of LB media and grown at 37°C until the culture reached an optical density at 600 nm of 0.7 absorbance units. At that point, protein expression was induced with 0.5 mM Isopropyl β-D-1-thiogalactopyranoside (IPTG) at 25°C for four hours. Cells were harvested by centrifugation at 4,000 r.p.m. for 30 minutes.

To express the p53CT protein with selenomethione instead of the endogenous sulfurmethionine, I followed the established protocol from Van Duyne *et al.* Instead of LB media, M9 minimal media with Na_2HPO_4 , KH_2PO_4 , NaCl , and NH_4Cl was used. Sterile 20% glucose, MgSO_4 , and CaCl_2 were also added to the culture. Protein expression proceeded in the presence of amino acids that inhibit methionine biosynthesis (lysine hydrochloride, threonine, phenylalanine, leucine, isoleucine, and valine) along with the addition of selenomethione.

Purification

Cell pellets were resuspended in a lysis buffer containing 150 mM NaCl and 50 mM Tris-base (pH 7.0). Cells were lysed with homogenizer and two cell disruption cycles in a french press in the presence of 0.04mM of the protease inhibitor phenylmethanesulfonyl fluoride (PMSF). The resulting cell lysate was centrifuged at 30,000 r.p.m. for 30 minutes to separate the soluble from the insoluble fraction. The soluble fraction was mixed with the amylose resin and incubated with gentle stirring for one hour in the cold room. The fusion protein MBP-pp-p53CT was bound to the amylose in the affinity column. At room temperature, the resin was extensively washed with lysis buffer and with high salt buffer 750mM NaCl and 50mM Tris-base (pH7.0) to eliminate non-specific binding. In the final step, the fusion MBP-pp-p53CT protein was eluted with lysis buffer containing 50mM of maltose.

Eluted fractions were digested overnight with PreScission protease in the cold room and proteolysis was confirmed with a 15% SDS-PAGE (Figure 2.3). The digested MBP fraction (MW 41.9kDa) appears at the level of the 43 kDa protein marker and the 8.5 kDa p53CT protein migrates in between the 10 and 17 kDa protein markers. As p53CT is positively charged with an isoelectric point of 8.35, it runs with a higher apparent molecular weight than expected due to its positive charges.

By using the difference in the isoelectric points of MBP (5.05) and p53CT (8.35), a cation exchanger column (Mono S) was used to separate the two proteins. In the 150mM NaCl and 50mM Tris-base (pH 7.0) buffer used, p53CT is positively charged and binds to the negatively charged Mono S column, while MBP on the other hand, is negatively charged and flows through the column without binding. The bound protein is eluted with a high salt step gradient of 250 mM, 500 mM, and 1M NaCl (Figure 2.4).

From a previous study of this construct in our lab by a former graduate student, Nikki Cheung, it was observed that the flexible loop region between the two domains underwent a non-specific proteolysis during crystallization. Proteolysis occurred between the Glu/Ala residues where the PreScission protease cleaved non-specifically. To avoid the non-specific proteolysis during crystallization, after the digestion step I raised the pH of the buffer from the optimal pH of 7 for the PreScission protease to 8.5 where the protease is less active. Even when the theoretical isoelectric points of the proteins predicted that using a buffer with pH 8.5 would not allow p53CT to bind to the ion exchange

Mono S column, the column continued to behave as when I used the pH 7 buffer with p53CT binding and MBP flowing through. For further experiments, the pure protein was desalted using a Sephadex G25 gel filtration column with a 50 mM NaCl and 20mM Tris base (pH 8.5) buffer (Figure 2.5). MALDI-TOF mass spectrometry was used to confirm the purity and the correct molecular weight of the protein (Figure 2.6).

To purify the proteins with incorporated selenomethione (Se-Met), I followed the same purification protocol as for the wild type. By again using MALDI-TOF, the incorporation of Se-MET was confirmed by observing the shift in the molecular weight of the protein from 8520.78 Da for the wild type p53CT to 8610.64 Da for the protein with Se-Met incorporated (Figure 2.7). The difference in the molecular weight of sulfur (32.07 Da) and selenium (78.96 Da) is 46.89 Da and the difference of 89.86 Da that I found closely corresponds to the expected difference for a protein, like p53CT, that contains two methionines. All Se-Met incorporated proteins were also purified with a pH 8.5 buffer after the PreScission protease digestion.

Crystallization

1.76 mM of pure Se-MET protein was mixed with 2.78 mM of 12 base pair p53 consensus DNA 5'-CGGGCATGCCCG-3'. This DNA was chosen because it was previously used for crystallizing with the p53 DNA binding domain. Crystallization trays were set up by the hanging drop vapor diffusion method at

23°C. The initial crystallization screening was carried out with preparations of the pure wild type protein. Crystallization screening solutions used were Crystal Screen I, PEG-ion screen, and PEG-pH screen designed by Hampton Research. The final optimized crystallization condition for p53CT was 20-22% polyethylene glycol 3350 (PEG 3350), 0.1M Tris-Base (pH 8.0-8.5), and 90-110 mM $\text{CaCl}_2 \cdot 2\text{H}_2\text{O}$. Once the crystallization condition was optimized, crystals were grown with Se-Met p53CT proteins. Crystals appeared as thin elongated rods after 10 days (Figure 2.8).

X-ray diffraction data collection and processing

To avoid ice formation, crystals were covered with Paratone-N (Hampton Research) as a cryoprotectant and were frozen and stored in liquid nitrogen before data collection. X-ray intensity data collection was done at Berkeley Advance Light Source. Diffraction data were collected using the ADSC Quantum-315R CCD detector on the BL 5.02 beam line. Crystals were maintained at 100 K during data collection. The crystal-to-detector distance was set to 400 mm. A MAD (Multiple Anomalous Diffraction) data set was collected corresponding to the maximum f_{00} (peak, 0.97891 Å), the minimum f_0 (edge, 0.97934 Å) and a reference wavelength (remote, 0.97 Å) chosen on the basis of the absorption spectrum of the Selenium atom. The diffraction data were processed with the HKL 2000 package. The crystal diffracted to 3.3 Å resolution and the crystal belongs to the trigonal system P3 with the unit cell parameters $a = b = 49.603$ Å,

$c = 92.95 \text{ \AA}$, $\gamma = 120.0^\circ$. p53CT consists of two Se-Met for each molecule and the solvent content suggested 12 molecules in the asymmetric unit with 24 Se-Met sites. Two Se-Met sites in the structure were obtained with the program SOLVE and these peaks were further refined using RESOLVE. Using the two known sites and the previously solved structure from our lab as a model for molecular replacement, we could solve the structure using PHENIX crystallographic program (Figure 2.10a, b). The structure was solved and refined to $R_{\text{cryst}}/R_{\text{free}}$ 0.26/0.36. The structure consists of 12 dimers of p53 tetramerization domain (323-353) each containing one Se-Met site. The structure was refined and omit-maps were calculated in order to check whether we could see the density for the regulatory domain (354-393). The unit cell packing showed that we could only crystallize the p53 tetramerization domain (323-353) (Figure 2.11).

Further the structure of p53CT (323-353) was refined with the programs suite PHENIX. The refinement calculations were interleaved with several rounds of model building with program coot. The refinement statistics are shown in Table 2.1. Postdoctoral fellow Abdul S. Ethayathulla took charge of data collection and processing.

Results

The p53CT protein crystallized in a P3 trigonal space group and a data set was collected with diffraction to a resolution of 3.3 \AA (Figure 2.9). The unit cell contains three asymmetric units and each asymmetric unit has 24 monomers of

the tetramerization domain (Figure 2.11). The 24 monomers in the asymmetric unit are arranged as four tetramers and four dimers that also form tetramers with symmetry related dimers. Although the P3 space group was different from the P6 crystals previously obtained by Nikki Cheung in our laboratory, the crystal also had the cleaved tetramerization domain, and the regulatory domain was absent. This indicates that again during the crystallization process the protein was cleaved between the tetramerization domain and the regulatory domain and only the tetramerization domain crystallized.

The solved structure showed 30 amino acids of the tetramerization domain (residues 323-353) and it was identical to the structure of tetramerization domain previously solved in other laboratories and also in our laboratory in the work described in Nikki Cheung's thesis (Cheung, 2010). A monomer of the tetramerization domain is formed by one beta strand (a.a. 326-333), a hinge glycine residue at position 334, and an alpha helix (a.a. 335-353). The dimer is held together by a two-strand beta-sheet formed by the characteristic alternate hydrogen bond pattern from the main chain amine and carbonyl groups of each monomer, resulting in a classical beta-sheet conformation. Then, the hydrophobic side chains of Met 340 and Leu 344 in four alpha-helices from two dimers form the tetramer that can be described as a dimer of dimers (Figure 2.1a,b).

Discussion

The goal of my structural studies was to crystallize the regulatory domain of p53 in the presence of DNA. In my crystallization experiments, instead of obtaining the complex of the p53CT construct bound to DNA, I obtained the crystal structure of the tetramerization domain that had already been solved. I speculate that the non-specific cleavage of p53CT protein that resulted in the crystallization of the tetramerization domain alone might have been mediated by a protease distinct from that of the highly specific PreScission protease. The non-specific cleavage most likely occurred during crystallization when the protein molecules were in close proximity with each other due to the high protein concentration used, and the contaminant protease could work more readily. In order to inactivate all proteases present in the prep, we started to incorporate protease inhibitor cocktail mix (Sigma) in subsequent crystallization drops and we are planning to modify our purification protocol to avoid the presence of proteases.

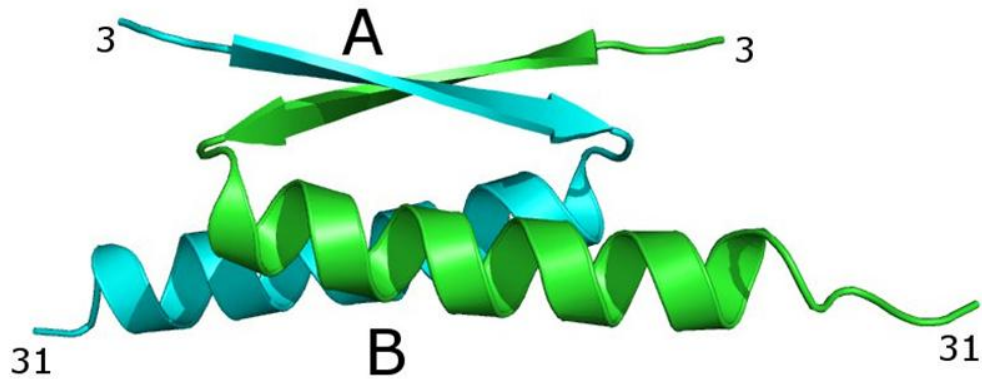


Figure 2.1a Dimer of p53CT Tetramerization Domain. The dimer contacts are mediated through the beta strands.

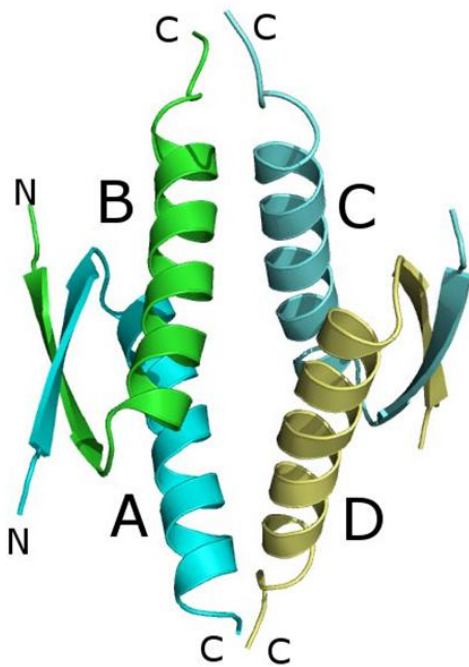
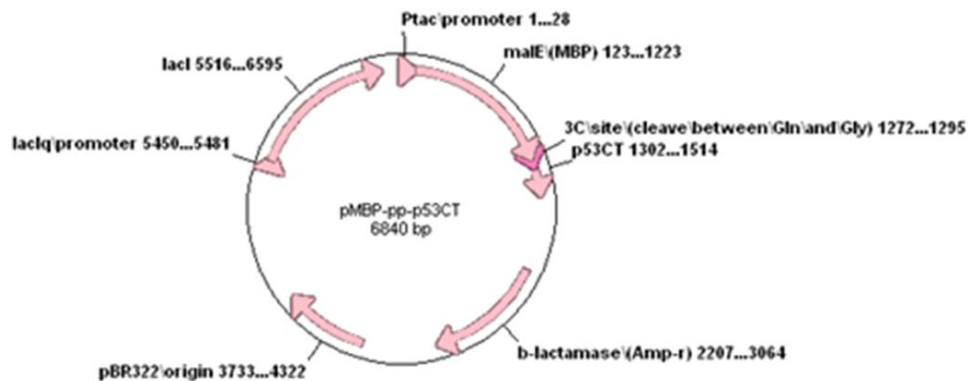


Figure 2.1b Tetramer of p53CT Tetramerization Domain. Tetramerization is mediated by the hydrophobic side chains lining the alpha helices. Two dimers come in contact to form the tetramer.



PreScission protease cleaves
Between Gln and Gly



Figure 2.2 p53CT construct. p53CT construct used in this thesis consists of the MBP fusion tag, a PreScission protease cleavage site, and the target protein. This construct was inserted into the pMAL expression vector. After cleavage, 43kDa MBP and 8.5kDa p53CT(TD+RD) separate on MonoS ion exchange column utilizing their charge differences.

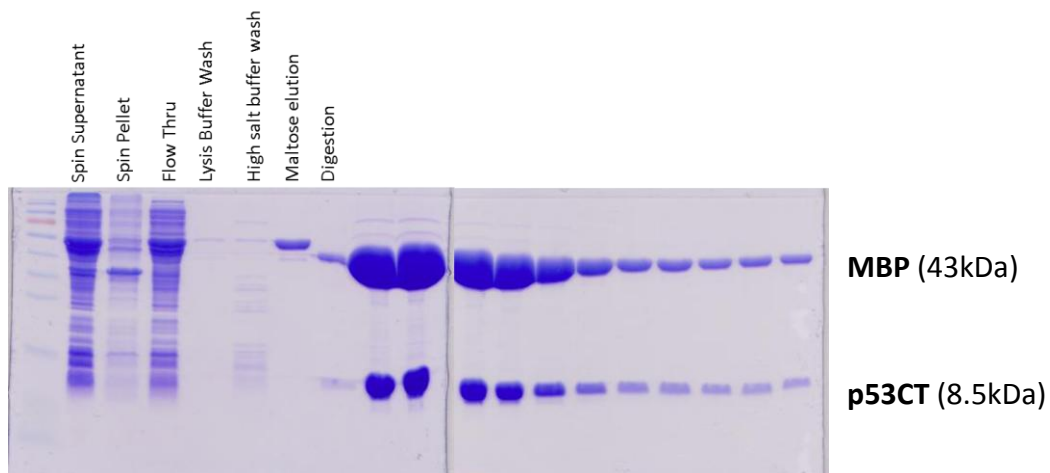


Figure 2.3 15% SDS-PAGE of p53CT expression and purification. p53 expression, purification, and digestion are shown. Elution before digestion is compared with digested fractions on the right.

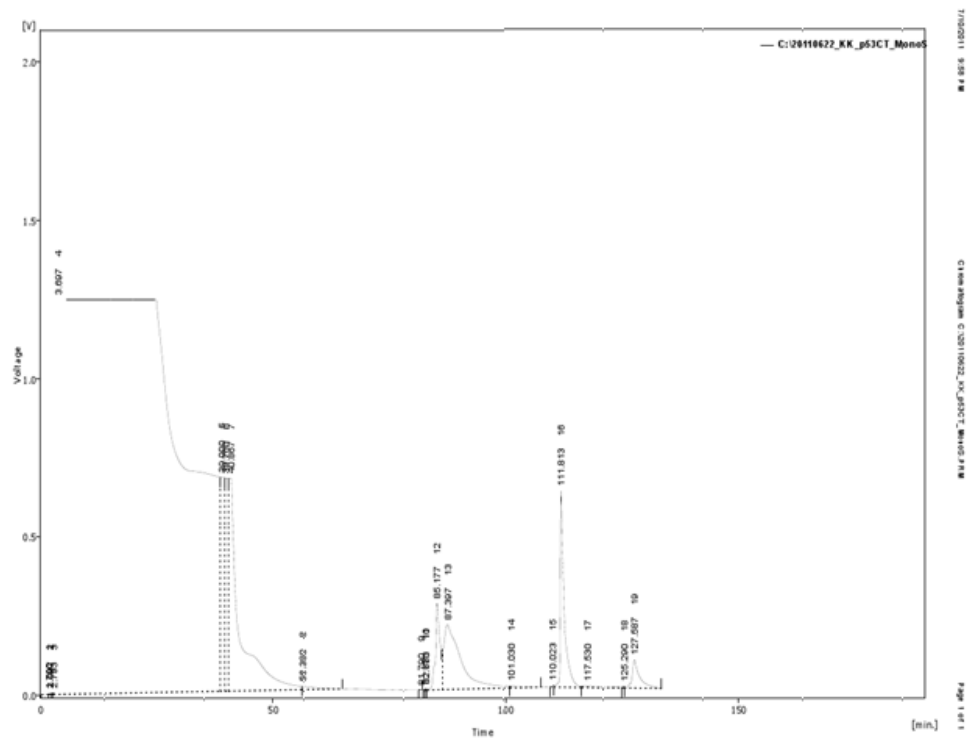


Figure 2.4 Mono S chromatography separating MBP (pI 5.05) from p53CT (pI 8.35). The first peak eluting out is the MBP peak, and the subsequent three peaks are the elutions of p53CT with 250mM NaCl, 500mM NaCl, and 1M NaCl with 50mM Tris-base at pH7.0.

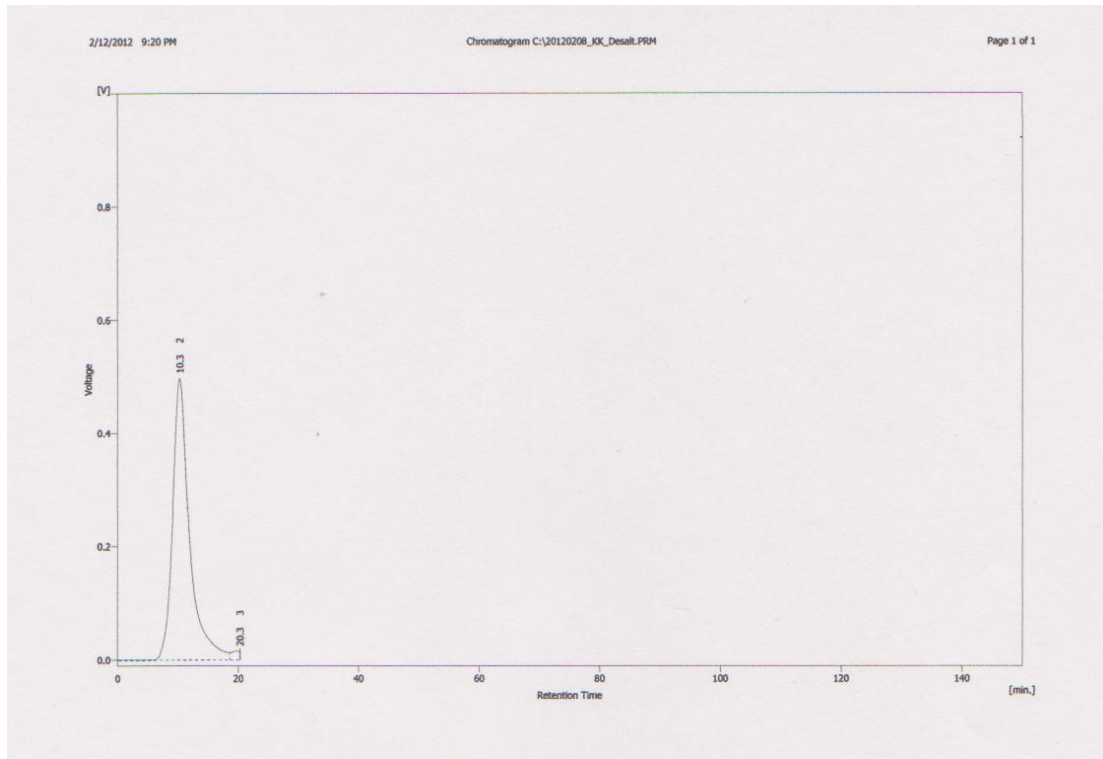


Figure 2.5 Desalt Chromatogram of pure p53CT concentrated and run on Sephadex 25. Pure fractions of p53CT from Mono S chromatography was concentrated and desalted as a single peak in 50 mM NaCl and 20mM Tris base (pH 8.5) buffer.

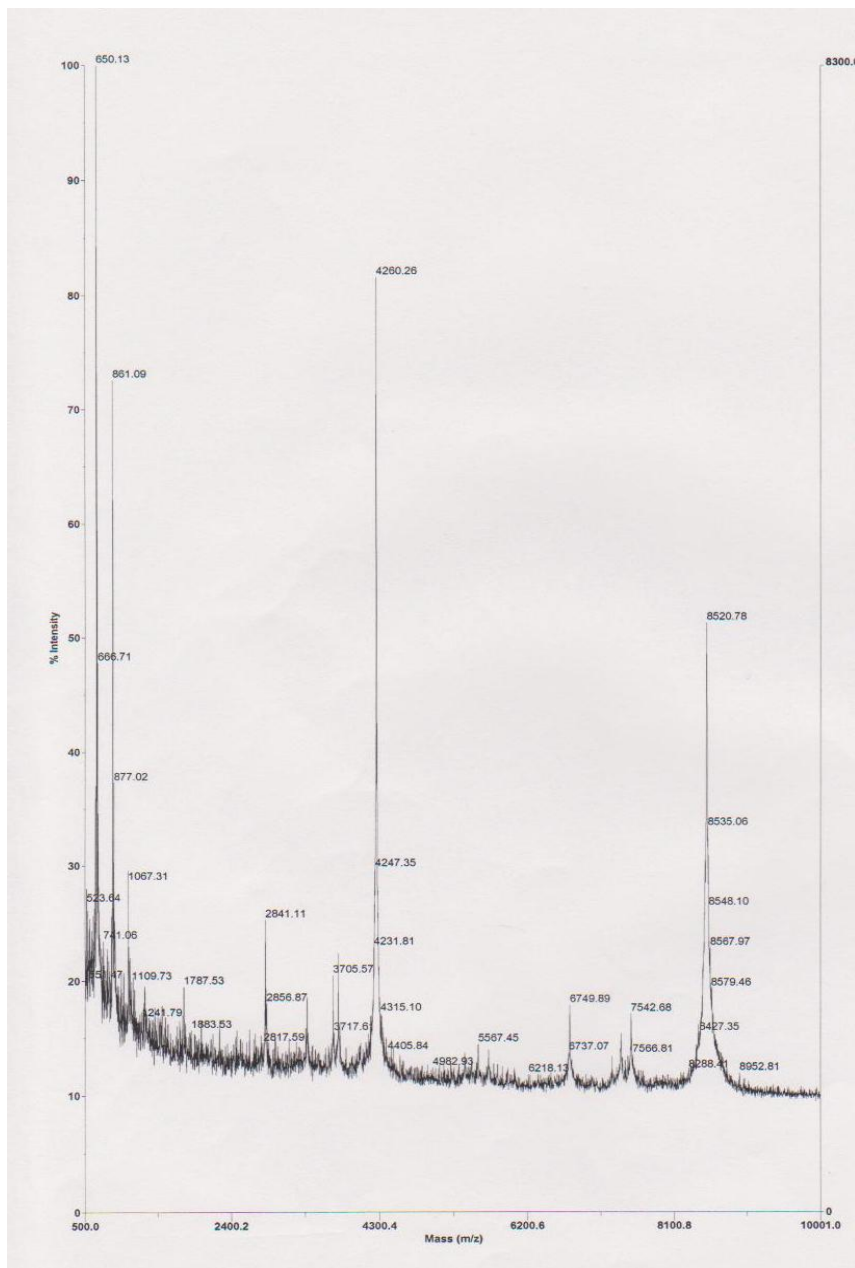


Figure 2.6 MALDI-TOF spectrum of p53CT wildtype protein. 75 amino acid construct has a theoretical molecular weight of 8524.66Da. Experimental molecular weight of 8520.78Da on the spectrum corresponds well to the theoretical value.

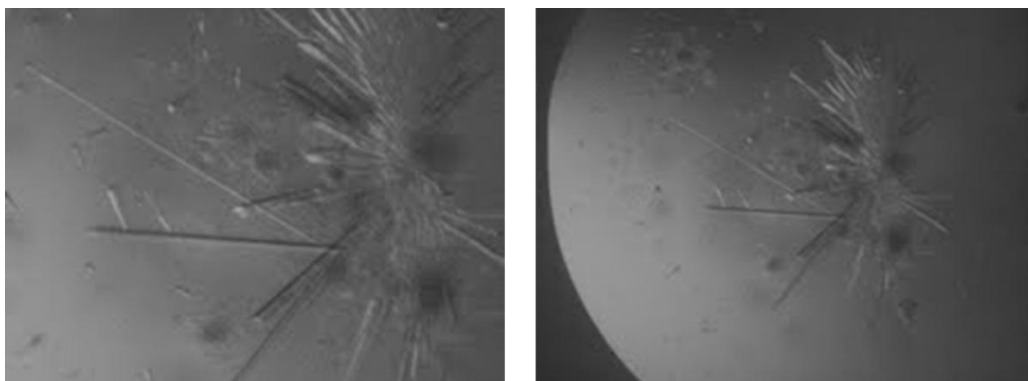


Figure 2.8 Se-MET incorporated p53CT protein crystals. Crystals were prepared with hanging drop vapor diffusion method with the condition 20-22% polyethylene glycol 3350 (PEG 3350), 0.1M Tris-Base pH 8.0-8.5, and 90mM-110mM $\text{CaCl}_2 \cdot 2\text{H}_2\text{O}$.

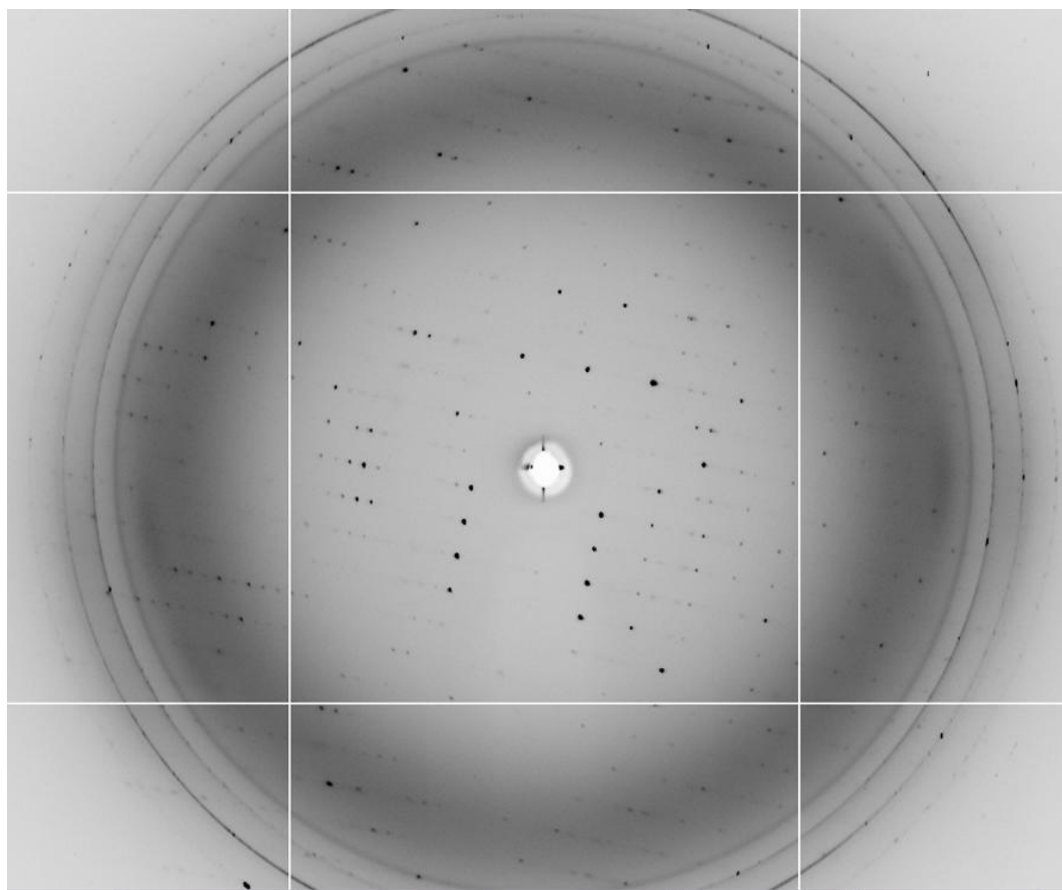


Figure 2.9 X-ray diffraction pattern of Se-MET incorporated p53CT. Crystal diffracted to 3.3 Å. Rod-shaped crystal belongs to the P3 trigonal space group.

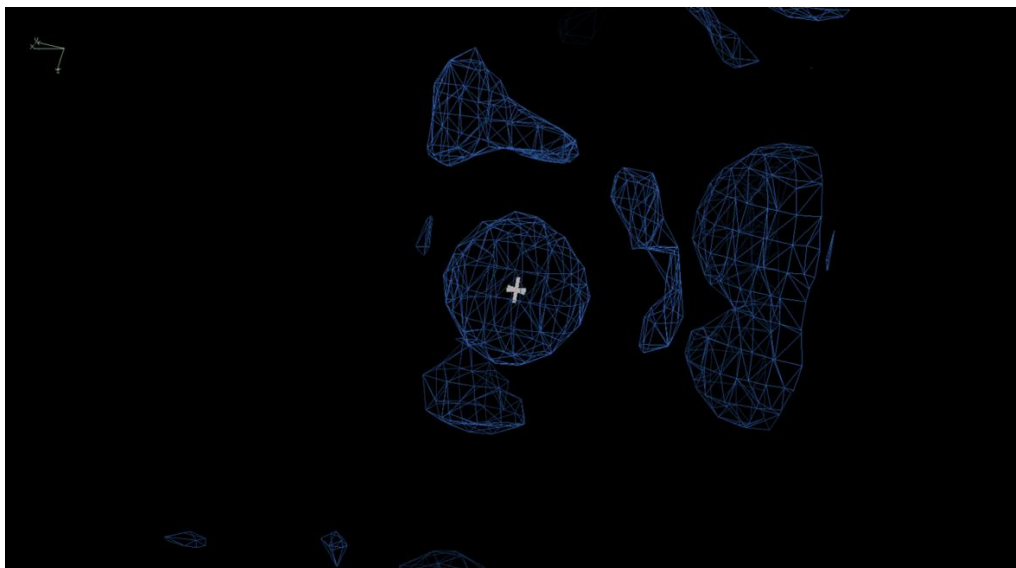


Figure 2.10a Electron density of Se-MET observed by the MAD method. The cross inside the electron density map represents the location of the selenium atom in Se-MET.

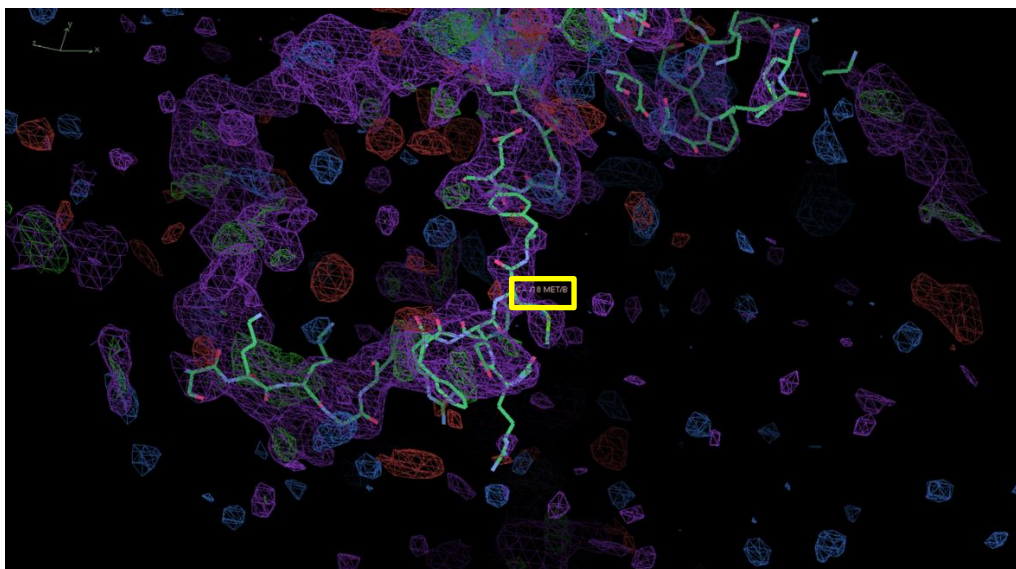


Figure 2.10b Building of the p53CT structure starting from the Se-MET site. The model was built from the Se-MET site with reference to the previous structure of the tetramerization domain solved. Se-MET site is boxed in yellow.

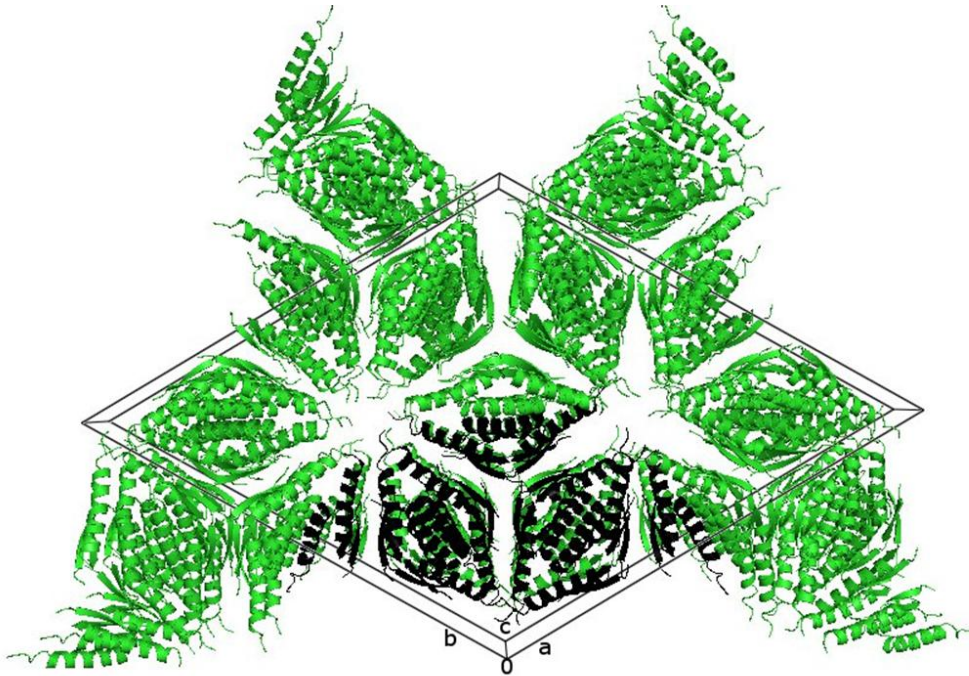


Figure 2.11 Unit cell packing of p53CT crystal. The unit cell belongs to the P3 trigonal space group with $\alpha=90$, $\beta=90$, $\gamma=120$. In one asymmetric unit indicated in black, there are 24 monomers of the tetramerization domain. They make up four tetramers and four dimers.

Table 2.1 Refinement table of p53CT structure. Summary of the information from the refinement of the p53 tetramerization domain.

Data collection		Refinement	
Space group	P3 Trigonal	Resolution (Å)	45.0 – 3.3
Cell dimensions		No. reflections	14627
a = b, c (Å)	137.039	Rwork / Rfree	26.2 / 36.3
	49.49	No. atoms	6448
	120	Protein	3467
		9B-factors	21.9
Resolution (Å)	50 – 3.3	Protein	70
		R.m.s. deviations	
Rsym or Rmerge	6(45)	Bond lengths (Å)	0.011
I / σI	8.7 (2.0)	Bond angles (°)	1.4
Completeness (%)	99.6(99.6)		
Redundancy	3.1	Most favored region	83.38
		Additionally allowed	16.62

References

Ayed, A.; Mulder, F. A.; Yi, G. S.; Lu, Y.; Kay, L. E.; Arrowsmith, C. H., Latent and active p53 are identical in conformation. *Nature structural biology* 2001, 8 (9), 756-60.

Chen, C.; Gorlatova, N.; Kelman, Z.; Herzberg, O., Structures of p63 DNA binding domain in complexes with half-site and with spacer-containing full response elements. *Proceedings of the National Academy of Sciences of the United States of America* 2011, 108 (16), 6456-61.

Chen, Y.; Dey, R.; Chen, L., Crystal structure of the p53 core domain bound to a full consensus site as a self-assembled tetramer. *Structure* 2010, 18 (2), 246-56.

Cheung, N. H. L., Biophysical characterization of p53 regulatory domain and MDM2. University of California, San Diego, La Jolla, 2010; pp. 1 online resource (xiii, 85 leaves) col. ill. <http://wwwlib.umi.com/cr/fullcit?p1477891>.

Cho, Y.; Gorina, S.; Jeffrey, P. D.; Pavletich, N. P., Crystal structure of a p53 tumor suppressor-DNA complex: understanding tumorigenic mutations. *Science* 1994, 265 (5170), 346-55.

Cross, B.; Chen, L.; Cheng, Q.; Li, B.; Yuan, Z. M.; Chen, J., Inhibition of p53 DNA binding function by the MDM2 protein acidic domain. *The Journal of biological chemistry* 2011, 286 (18), 16018-29.

Emamzadah, S.; Tropia, L.; Halazonetis, T. D., Crystal structure of a multidomain human p53 tetramer bound to the natural CDKN1A (p21) p53-response element. *Molecular cancer research : MCR* 2011, 9 (11), 1493-9.

Ho, W. C.; Fitzgerald, M. X.; Marmorstein, R., Structure of the p53 core domain dimer bound to DNA. *The Journal of biological chemistry* 2006, 281 (29), 20494-502.

Kaesler, M. D.; Iggo, R. D., Chromatin immunoprecipitation analysis fails to support the latency model for regulation of p53 DNA binding activity in vivo. *Proceedings of the National Academy of Sciences of the United States of America* 2002, 99 (1), 95-100.

Kitayner, M.; Rozenberg, H.; Kessler, N.; Rabinovich, D.; Shaulov, L.; Haran, T. E.; Shakked, Z., Structural basis of DNA recognition by p53 tetramers. *Molecular cell* 2006, 22 (6), 741-53.

Kitayner, M.; Rozenberg, H.; Rohs, R.; Suad, O.; Rabinovich, D.; Honig, B.; Shakked, Z., Diversity in DNA recognition by p53 revealed by crystal structures

with Hoogsteen base pairs. *Nature structural & molecular biology* **2010**, 17 (4), 423-9.

Levine, A. J., p53, the cellular gatekeeper for growth and division. *Cell* **1997**, 88 (3), 323-31.

Malecka, K. A.; Ho, W. C.; Marmorstein, R., Crystal structure of a p53 core tetramer bound to DNA. *Oncogene* **2009**, 28 (3), 325-33.

Ou, H. D.; Lohr, F.; Vogel, V.; Mantele, W.; Dotsch, V., Structural evolution of C-terminal domains in the p53 family. *The EMBO journal* **2007**, 26 (14), 3463-73.

Riley, T.; Sontag, E.; Chen, P.; Levine, A., Transcriptional control of human p53-regulated genes. *Nature reviews. Molecular cell biology* **2008**, 9 (5), 402-12.

Rustandi, R. R.; Baldisseri, D. M.; Weber, D. J., Structure of the negative regulatory domain of p53 bound to S100B(beta-beta). *Nature structural biology* **2000**, 7 (7), 570-4.

Van Duyne, G. D.; Standaert, R. F.; Karplus, P. A.; Schreiber, S. L.; Clardy, J., Atomic structures of the human immunophilin FKBP-12 complexes with FK506 and rapamycin. *Journal of molecular biology* **1993**, 229 (1), 105-24.

Weinberg, R. L.; Freund, S. M.; Veprintsev, D. B.; Bycroft, M.; Fersht, A. R., Regulation of DNA binding of p53 by its C-terminal domain. *Journal of molecular biology* **2004**, 342 (3), 801-11.

Weinberg, R. L.; Veprintsev, D. B.; Fersht, A. R., Cooperative binding of tetrameric p53 to DNA. *Journal of molecular biology* **2004**, 341 (5), 1145-59.

Chapter Three

Functional Characterization of the

p53 C-terminus: p53CT DNA

Binding

Introduction

p53 has two domains that bind DNA. The central DNA binding domain binds upstream of the p53 target genes where there are two 10 bp half-sites with the following consensus sequence: PuPuPuC(A/T)(A/T)GPyPyPy (Pu=Purine, Py=Pyrimidine). The DNA binding domain binds to this “specific” response element as a dimer of dimers with nanomolar affinity (Weinberg, Freund *et al.*). And the C-terminal regulatory domain binds to DNA non-specifically with micromolar affinity (Weinberg, Freund *et al.*). The consensus response elements allow the transcription machinery to assemble upstream of the target genes and increase their rate of transcription, while the C-terminal regulatory domain is postulated to facilitate p53 sliding on DNA to efficiently locate the response elements.

Due to the lack of structural knowledge on the regulatory domain, the role of the p53 C-terminus in transactivation mechanism remains unexplained. The mechanism of action of the p53 regulatory domain is described as sliding on the DNA until it finds the target response element. To carry out such a role, binding to DNA has to be non-specific to allow free movement along the DNA phosphate backbone (Weinberg, Freund *et al.*). Once the response element is located, then the residues in the DNA binding domain recognize the DNA bases with nanomolar affinity (Weinberg, Freund *et al.*). The specific recognition to DNA has been well described with numerous crystal structures (Chen *et al.*, Cho *et al.*,

Emamzadah *et al.*, Ho *et al.*, Kitayner *et al.*, Malecka *et al.*), but the non-specific recognition has not been structurally defined.

The recognition of DNA by the regulatory domain remains unanswered due to the difficulty of elucidating the structure of a region that is predicted to be highly flexible. The regulatory domain can adopt a stable secondary structure upon binding to other proteins, and probably upon ligand binding such as DNA. In order to form a p53CT-DNA complex for crystallization, we wanted to identify a DNA molecule that is more likely to promote crystallization. For this purpose, we analyzed by sedimentation velocity experiments the ability of p53CT to bind a panel of oligonucleotides with different lengths and sequences. Again, the final goal of the biophysical characterization of DNA binding by p53CT is to help the crystallization efforts described in Chapter 2.

We also created a p53CT M340Q-L344R double mutant that is expected to only form dimers, instead of tetramers, because the mutations abolish the hydrophobic interactions that mediate tetramerization. We set out to test the DNA binding properties of the double mutant to consider the feasibility of its crystallization. We reasoned that the crystal structure of this mutant with DNA would shed light on the true symmetry of the tetramerization domain (TD) upon DNA binding, because for the moment, the D2 symmetry observed for the 30 amino acids structure of the tetramerization domain is in conflict with the better established C2 symmetry of the DNA binding domain when it is bound to the DNA. Alternatively, we also created p53CT acetylation mutants where the six

lysines in the regulatory domain prone to be acetylated (K370, K372, K373, K381, K382, K386) were mutated to glutamine to mimic acetylation. Chemical shift changes in the NMR spectra of p53CT after DNA binding indicate that five of these residues (K370, K373, K381, K382, K386) are important in DNA binding (Weinberg, Freund *et al.*). By characterizing these mutants, our goal is to help the future crystallization experiments.

Materials and Methods

Analytical Ultracentrifugation

For the sedimentation velocity experiments, pure p53CT at a concentration that gave an absorbance reading at 280 nm of 0.1 AU or greater was required. It was equilibrated with the DNA to be tested for one hour at 20°C inside the analytical ultracentrifuge. Each analytical ultracentrifuge cell contains two optical paths, one was used as the reference with 400 μ l of buffer 100 mM NaCl and 20 mM Na₂HPO₄ (pH 7.0). The adjacent optical path had the p53CT-DNA complex in the same buffer where 0.15mg of protein and 10.5ug of DNA were added. Sedimentation of the protein-DNA complex was followed by the absorbance of the fluorescein label at 488 nm. Sedimentation velocity experiments were run at 41,000 r.p.m. and at 20°C constant temperature. These experiments were carried out by a former graduate student Nikki Cheung in our

lab. Software Sedfit (NIH) was used to analyze the data and to calculate the sedimentation coefficient and the molecular weight of the sedimenting species.

Cloning and Purification of the p53CT Dimer Mutant

A QuickChange mutagenesis (Stratagene) protocol with the wild type p53CT plasmid as the template was used to create the double mutant p53CT M340Q-L344R. The PCR reaction was digested with the restriction endonuclease *DpnI* before transforming XL-1 Blue competent cells with only the newly synthesized vectors that included the mutant gene. After verifying the new sequence, I followed the same purification protocol for the wild type p53CT described in Chapter 2.

Cloning and Purification of the p53CT Acetylation Mutant

The QuickChange mutagenesis (Stratagene) was also used to introduce two sets of triple mutants in the p53CT constructs. One set had K370Q, K373Q and K373Q for both the wild type and the dimer mutant proteins, and another set had K381Q, K382Q and K386Q also for both the wild type and the dimer mutant proteins. Lastly, two other mutants containing all six lysine-to-glutamine mutants were created for the wild type and the dimer mutant proteins. After transforming XL-1 blue competent cells with the mutant vectors and verifying the correct

sequences, these mutants were expressed in BL21(DE3) cells and purified according to the wild type protein protocol outlined in Chapter 2.

Results

p53CT binds to both specific and non-specific DNA as a tetramer

As a control of our analysis to verify the formation and the oligomerization state of the p53CT-DNA complexes, we first determined the sedimentation coefficient for all of the double stranded DNAs utilized that were in the range between 8 to 32 bp (Table 3.1). As can be seen in Figure 3.1, there is a positive correlation between the DNA length and the sedimentation coefficient with a confidence level greater than 95%. As expected, as the molecular weight becomes larger the sedimentation coefficient increases.

In Table 3.2 we observe that with the increase in DNA length, there is an increase in the sedimentation coefficient value of the complex species (DNA bound to p53CT) for both the specific and the non-specific DNAs (last two rows in Table 3.2 belong to the sequences different from the consensus RE, I call these sequences non-specific DNAs. Sequences of the DNA are listed in Tables 3.3 and 3.4). For DNA length 8bp to 16bp, the experimental molecular weight of the complex agrees well with the theoretical molecular weight calculated for one tetramer of p53CT bound to the dsDNA. However, starting with the 20 bp DNA, the experimental molecular weight of the complex gets significantly larger than

the theoretical molecular weight of one tetramer of p53CT bound to the dsDNA. This indicates that the DNA molecules equal or greater than 20 bp can accommodate a second p53CT tetramer. This observation is confirmed for the non-specific DNAs shown in the last two rows of Table 3.2. The experimental value however, does not exactly reach the two tetramers bound to the dsDNA (Table 3.2). It is postulated that the intermediate value seen between one tetramer and two tetramers bound to the DNA is due to the weak micromolar binding of the tetramer to the DNA. During sedimentation the protein is on and off the DNA producing a molecular weight that is lower than what it would be expected for a tighter complex. This results in an intermediate sedimentation coefficient.

Discussion

To search for the DNA sequence of its response elements, p53 slides along the DNA. It has been observed that p53 shows this behavior only when the C-terminus is present, where p53 uses the regulatory domain to scan along the DNA making weak contacts with the DNA phosphate backbone. From this model it is thought that the regulatory domain should not have a specific binding towards DNA. Our experiments demonstrated the lack of DNA specificity because p53CT binds in very similar ways to both the specific and the non-specific DNAs. It would be important to further study the binding with fluorescent

anisotropy to obtain more quantitative data on the regulatory domain binding to DNA.

I learned from the sedimentation velocity experiments that p53CT binds DNA as a tetramer. It would be interesting to confirm this binding structurally to gain mechanistic insight into the role of the regulatory domain in tumor suppression.

Lastly, results from the dimer mutant and the acetylation mutants I have been working on are not reported in this thesis because I am still establishing their purification protocols. However, DNA binding studies and further crystallization with these mutants may help us to better understand the symmetry, as well as the DNA binding mechanism of the regulatory domain.

Table 3.1 Sedimentation Coefficients of Various DNAs. Experimental M.W. of the DNAs correspond well with the theoretical M.W.. As the length of the double stranded DNA increases, the sedimentation coefficient also increases.

DNA	Sequence 5'-3'	Sedimentation Coefficient [S]	rmsd	Experimental M.W. (kDa)	Theoretical M.W. (kDa)
8bp	GGCATGCC	1.34	0.006503	5.82	5.31
10bp	GGGCATGCCC	1.32	0.006356	7.99	6.55
12bp	TGGGCATGCCCA	1.57	0.006741	7.43	7.78
14bp	ATGGGCATGCCCAT	1.41	0.005179	7.45	9.02
16bp	GCATGCCCGGGCATGC	1.60	0.006014	10.2	10.26
20bp	GGGCATGCCCGGGCAT GCC	1.90	0.007095	12.8	12.73
24bp	TCGGGCATGCCCGGGC ATGCCCGA	2.19	0.006305	14.7	15.20
28bp	TGTCGGGCATGCCCGG GCATGCCCGACA	2.63	0.006870	17.6	17.67
32bp	TATGTCGGGCATGCC GGGCATGCCCGACATA	2.68	0.006479	18.4	20.14

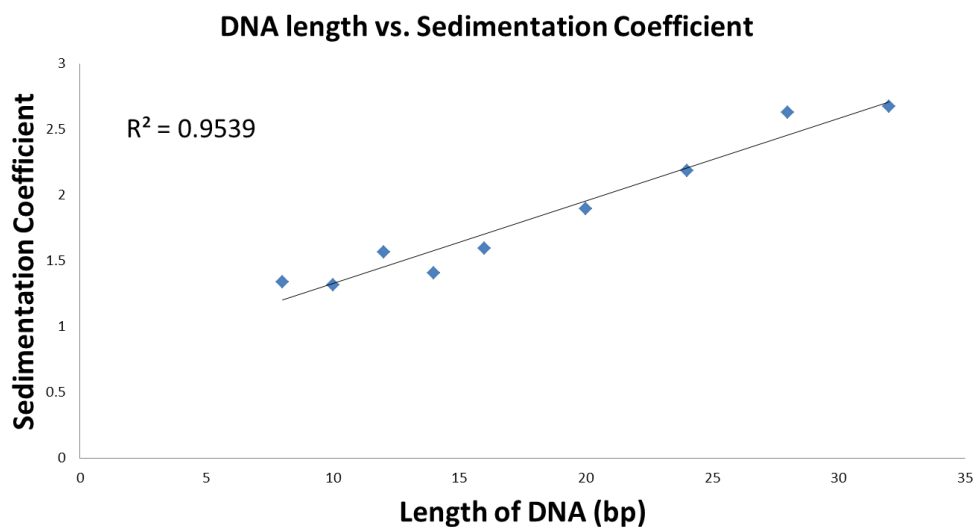


Figure 3.1 DNA length vs. Sedimentation coefficient. There is a positive correlation between the length of DNA and the sedimentation coefficient.

Table 3.2 Summary of sedimentation velocity experiments with specific and non-specific DNAs. Experimental molecular weight of the complex for specific (blue rows) and non-specific (pink rows) DNAs with p53CT are compared with the theoretical values to determine the oligomerization of the sedimenting species.

DNA	Complex [S]	rmsd	Experimental M.W. of complex (kDa)	Theoretical M.W. of Tetramer+DNA (kDa)	Theoretical M.W. of 2x Tetramer +DNA (kDa)	Conclusion
8	2.58	0.00554	40.8	40.52	75.22	tetramer
10	3.07	0.00635	42.8	42.69	77.39	tetramer
12	2.63	0.00574	41.4	42.13	76.83	tetramer
16	2.68	0.00570	42.5	44.90	79.60	tetramer
20	3.49	0.00591	59.4	47.50	82.20	mixture
24	3.83	0.00688	75.3	49.40	84.10	mixture
28	4.13	0.00614	77.3	52.30	87.00	mixture
20	3.63	0.00526	64.2	47.50	82.20	mixture
24	3.30	0.00517	65.4	49.40	84.10	mixture

Table 3.3 Specific DNA sequences. Specific DNA sequences contain the consensus response element sequence that is recognized by the DNA binding domain.

Specific DNA (bp)	Sequence 5'-3'
8	GGCATGCC
10	GGGCATGCCC
12	TGGGCATGCCCA
16	GCATGCCCGGGCATGC
20	GGGCATGCCCGGGCATGCCC
24	TCGGGCATGCCCGGGCATGCCCGA
28	TGTCGGGCATGCCCGGGCATGCCCGACA

Table 3.4 Non-specific DNA sequences. Non-specific DNA sequences do not contain the consensus response element sequence recognized by the DNA binding domain.

Non-specific DNA (bp)	Sequence 5'-3'
20	CCCGTACGGGCCCGTACGGG
24	TCCCCGTACGGGCCCGTACGGGGA

References

- Ayed, A.; Mulder, F. A.; Yi, G. S.; Lu, Y.; Kay, L. E.; Arrowsmith, C. H., Latent and active p53 are identical in conformation. *Nature structural biology* 2001, 8 (9), 756-60.
- Chen, Y.; Dey, R.; Chen, L., Crystal structure of the p53 core domain bound to a full consensus site as a self-assembled tetramer. *Structure* 2010, 18 (2), 246-56.
- Cheung, N. H. L., Biophysical characterization of p53 regulatory domain and MDM2. University of California, San Diego, La Jolla, 2010; pp. 1 online resource (xiii, 85 leaves) col. ill. <http://wwwlib.umi.com/cr/fullcit?p1477891>.
- Cho, Y.; Gorina, S.; Jeffrey, P. D.; Pavletich, N. P., Crystal structure of a p53 tumor suppressor-DNA complex: understanding tumorigenic mutations. *Science* 1994, 265 (5170), 346-55.
- Emamzadah, S.; Tropia, L.; Halazonetis, T. D., Crystal structure of a multidomain human p53 tetramer bound to the natural CDKN1A (p21) p53-response element. *Molecular cancer research : MCR* 2011, 9 (11), 1493-9.
- Ho, W. C.; Fitzgerald, M. X.; Marmorstein, R., Structure of the p53 core domain dimer bound to DNA. *The Journal of biological chemistry* 2006, 281 (29), 20494-502.
- Kitayner, M.; Rozenberg, H.; Kessler, N.; Rabinovich, D.; Shaulov, L.; Haran, T. E.; Shakked, Z., Structural basis of DNA recognition by p53 tetramers. *Molecular cell* 2006, 22 (6), 741-53.
- Levine, A. J., p53, the cellular gatekeeper for growth and division. *Cell* 1997, 88 (3), 323-31.
- Malecka, K. A.; Ho, W. C.; Marmorstein, R., Crystal structure of a p53 core tetramer bound to DNA. *Oncogene* 2009, 28 (3), 325-33.
- Rustandi, R. R.; Baldisseri, D. M.; Weber, D. J., Structure of the negative regulatory domain of p53 bound to S100B(beta-beta). *Nature structural biology* 2000, 7 (7), 570-4.
- Weinberg, R. L.; Freund, S. M.; Veprintsev, D. B.; Bycroft, M.; Fersht, A. R., Regulation of DNA binding of p53 by its C-terminal domain. *Journal of molecular biology* 2004, 342 (3), 801-11.

Weinberg, R. L.; Veprintsev, D. B.; Fersht, A. R., Cooperative binding of tetrameric p53 to DNA. *Journal of molecular biology* **2004**, 341 (5), 1145-59.

Chapter Four

Functional Characterization of the p53 C-terminus: Regulation by MDM2

Introduction

To characterize the p53 C-terminus, it is important to examine its interaction with MDM2. MDM2 protein is the principal negative regulator of p53 and it inactivates p53 by adding ubiquitin molecules to the C-terminus of p53. To function as an E3 ubiquitin ligase with p53 molecule as a substrate, MDM2 must use the C-terminal RING (Really Interesting New Gene) domain to form homo- or heterodimers with itself or with its homolog MDMX (Uldrijan *et al.*). The oligomerized RING domains recruit E2 conjugating enzymes that conjugate ubiquitin molecules into a chain. Then the E3 enzyme ligates the ubiquitin chain to the C-terminal Lys residues of p53 (Maki *et al.*). For this reason, investigating MDM2 has become an important area within the field of p53 research. It is important to study the MDM2 oligomerization to understand the interaction of MDM2 with the C-terminus of p53. Moreover, it has been shown that the C-terminus of p53 not only interacts with the MDM2 RING domain but also binds to the MDM2 N-terminus (Poyurovsky *et al.*).

In this thesis, I examined the oligomerization state of several MDM2 constructs. In addition to studying the wild type MDM2, I also studied a C-terminus deletion mutant. The last five amino acids of MDM2 are essential for oligomerization and E3 ligase activity, with Phe490 being the critical residue in both functions (Poyurovsky *et al.*). To understand how the MDM2 C-terminus stabilizes the RING structure to provide a binding platform for E2 enzymes, our aim was to obtain the monomers of the truncated mutant of MDM2 to study its

structure, as well as its interaction with p53. We also explored whether the presence of zinc could affect the oligomerization of the wild type MDM2 and its truncated mutant. We reasoned that zinc helps in proper folding of the protein and mediates oligomerization by coordinating cysteines in the zinc finger and the RING domains of MDM2, so its presence should be essential. We also created a fusion protein of MDM2 with MBP on the C-terminus to observe whether the bulky MBP tag would disrupt the oligomerization of MDM2. We also co-expressed MDM2 with MBP-p53CT in BL21 (DE3) cells and noted how the presence of p53CT affected the MDM2 oligomerization state.

MDM2 is a 491 amino acid protein with a 56 kDa molecular weight (Figure 4.1). Its N-terminal domain (residues 1-100) has a hydrophobic crevice that binds to the p53 N-terminus to inhibit p53 transactivation. The anti-cancer drug Nutlin is a cis-imidazoline analog that binds to the hydrophobic pocket normally occupied by p53 and disrupts the MDM2 inhibition of p53 (Lane *et al.*). Nuclear localization and nuclear export sequences (NLS and NES) in between residues 100-200 allow MDM2 to be carried by the import and export nuclear machinery across the nuclear membrane to target p53 for ubiquitination inside and outside of the nucleus (Lane *et al.*).

The acidic domain of MDM2 comprises residues 222 to 303 and includes sites for phosphorylation and for binding other proteins such as p14/p19, p300, and the ribosomal proteins L5, L11 and L23 (Lane *et al.*). The acidic domain regulates p53 through a ubiquitin-independent mechanism, where the MDM2

acidic domain binding to p53 DBD triggers a conformational change of the p53 DBD that inhibits p53's DNA binding activity (Cross *et al.*).

The zinc finger domain of MDM2, that covers residues 290 to 335, contains an important cysteine residue (C305) for protein folding that coordinates zinc. This domain also binds ribosomal proteins and is involved in the cellular response to ribosomal stress (Lane *et al.*).

Lastly, residues 429 to 491 form the RING domain. It is important in maintaining the overall structure through the conserved cysteine and histidine residues that bind two zinc atoms (Lane *et al.*). As mentioned before, the RING domain confers an important cellular function by assembling MDM2 into multimers.

Materials and Methods

Expression and Purification of Human MDM2

The pET28 bacterial expression vector containing the human MDM2 gene was inserted into the *Escherichia Coli* BL21(DE3) cells. Cells were grown in Yeast Tryptone (YT) media at 37°C until the OD₆₀₀ was approximately 0.6 AU. At that point, protein expression, under the control of the lac operon, was induced with 0.5 mM isopropyl β-D-1-thiogalactopyranoside (IPTG) for four hours at 25°C.

The harvested cells were re-suspended in a buffer with 500 mM NaCl, 50 mM Tris-base (pH 8.0) and 20 mM Imidazole. The cells were lysed with a homogenizer and two cell-disruption cycles in a french press in the presence of 0.2 mM of serine protease inhibitor phenylmethanesulfonylfluoride (PMSF). The soluble fraction of the lysed cells was separated from the insoluble fraction by centrifugation for 30 minutes at 30,000 r.p.m. Then, the soluble fraction was bound in batch with gentle stirring with Ni-NTA resin (QIAGEN) in the cold room at 4°C for one hour. A gravity column was set up with the protein-bound Ni-NTA resin and the cell lysate was flowed through the column. The column was extensively washed with lysis buffer (500 mM NaCl, 50 mM Tris-base (pH 8.0) and 20 mM imidazole), and later with the same buffer with 40 mM imidazole added to disrupt the non-specific binding of contaminant proteins to the Ni-NTA resin. Finally, the 6-His tagged MDM2 protein was eluted with a step gradient of 100 to 500 mM imidazole added to the initial lysis buffer.

Pure fractions were pooled together and concentrated before running a Superose 6 size exclusion chromatography column. The running buffer was the same as the lysis buffer with the similar imidazole concentration as the pooled fractions. The column was run at a 0.5 ml/min flow rate in all the experiments.

Purification of human MDM2 with zinc

When the effect of zinc was tested in the purification protocols, the steps were carried out in the same way as the above described preparation for the wild

type MDM2, with the exception of the addition of 0.1 mM ZnCl₂ in the elution buffers.

Cloning and Purification of the MDM2 truncated mutant MDM2ΔC7

The MDM2ΔC7 truncation mutant was created using the QuickChange mutagenesis method described by Stratagene. The forward and reverse oligonucleotides were designed to exclude the codons for the last seven amino acids of the wild type MDM2 gene in the pET28 vector. After the QuickChange PCR reaction, the total product was digested with *DpnI* to remove the wild type vector. The newly synthesized template carrying the mutation and the kanamycin resistant gene was used to transform the XL1-Blue cells. The transformed cells were grown on kanamycin plates and purified plasmids from several colonies were sequenced to confirm the success of the mutagenesis. The plasmid carrying the mutant MDM2 gene was used to transform the BL21 (DE3) cells. Expression and purification of the truncated mutant followed the same protocol as the wild type, and the effect of the presence of 0.1 mM ZnCl₂ was tested.

Cloning and Purification of the MDM2-MBP Construct

Due to the importance of the MDM2 C-terminal domain for oligomerization, the addition of a large tag in the C-terminus would be expected to interfere with the oligomerization by the C-terminal RING domain. To test if the bulky MBP tag could disrupt the oligomerization of MDM2 and result in the

monomeric MDM2, I cloned the MBP tag in the C-terminus of the MDM2 gene that already had a six-histidine tag in the N-terminus.

The recombinant gene construct was created using PCR with a template vector containing the MBP gene and primers that added *HindIII* and *XhoI* restriction endonuclease sites to the N and C-termini of MBP. The PCR product was digested with the restriction enzymes *HindIII* and *XhoI* at 37°C and purified with a PCR extraction kit (Bioneer). The same pET28 vector used for the expression of the wild type MDM2 was used in the digestion with *HindIII* and *XhoI* for 2 hours at 37°C. The digested plasmid was run on 1.2% agarose gel with ethidium bromide, and the high molecular weight band containing the MDM2 gene was sliced out of the gel and purified with an agarose gel purification kit (Bioneer). The purified digestion products of the MBP and MDM2 genes were ligated overnight at 14°C using the T4 DNA ligase. After sequencing the plasmid carrying the fusion protein, the QuickChange method described by Stratagene was used to introduce the amino acids GSGSG as a flexible linker between the MDM2 and MBP genes.

Purification of MDM2-MBP was achieved by the affinity MBP-tag purification using the amylose resin. Cells were re-suspended in a lysis buffer containing 500 mM NaCl, 50 mM Tris-base (pH 8.0) and 20 mM Imidazole with the addition of 0.2 M PMSF protease inhibitor to inhibit proteolysis. After homogenization and two cell disruption cycles in a french press, the lysed cells were centrifuged at 30,000 r.p.m. for 30 minutes at 4°C to remove the cell debris

and the membranous fraction. The soluble fraction was gently stirred with amylose resin for one hour in the cold room. An affinity column was set up with the batch bound resin, and the resin was extensively washed with the lysis buffer. Then, the fusion protein MDM2-MBP was eluted from the amylose column with the lysis buffer containing 50 mM maltose. After the presence of MDM2-MBP was confirmed in a western blot, the amylose column elutant was passed through the Superose 6 size-exclusion chromatography column with the lysis buffer at a 0.5ml/min flow rate.

Co-expression of MDM2 and p53CT

In our attempt to study the effect of p53CT binding to MDM2 *in vitro*, we transformed BL21 (DE3) expression cells with two vectors, one containing 6xHis-MDM2 and the other containing MBP-p53CT. I followed two affinity purification protocols, one using the Ni-NTA resin and the other using the amylose resin. First, the desired MDM2-p53CT complex was purified using the His-tag and the MDM2 purification method. In the other protocol, I approached purification using the MBP tag and the p53CT purification protocol. Purification protocols for His-tag and MBP-tag followed the same protocols as described previously for MDM2 and p53CT, respectively. After each respective tag purification, western blots were developed using anti-his and anti-MBP antibodies to detect the presence of both proteins in the preparation. For further purification, the elution fractions from the affinity columns were concentrated for superose 6 gel filtration chromatography.

Results

Wild type MDM2 oligomerization is not affected by 0.1 mM zinc

Human MDM2 protein has 491 amino acids and its molecular weight is 56 kDa. However, during electrophoresis in a 10% SDS-PAGE gel with heat and reducing agent, it migrates as a double band with a molecular weight close to the 95 kDa protein marker. This behavior is unexpected because the highly acidic protein with a theoretical pI of 4.72 should appear below the expected 56 kDa range due to its highly negative charges. The presence of a double band is also unusual because any effect of protein conformations should be disrupted by heating and the reducing conditions. Previously the identity of the double band as MDM2 had been confirmed by identifying the proteolytic fragments by ES-MS. From these data, it can be speculated that the double band may consist of a dimer of MDM2, which agrees with the molecular weight range of 90 kDa with consideration of the charge behavior that makes the acidic protein migrate lower in the gel (Figure 4.2, 4.3).

In size exclusion chromatography, I observed oligomers of MDM2 eluting around 55 minutes which corresponds to a molecular weight of ~669 kDa according to a calibrated column (Figure 4.4). Previous sedimentation velocity results from the thesis work of a former graduate student, Nikki Cheung (Cheung, 2010) (data not shown), show that MDM2 forms dimers, trimers, tetramers and hexamers in solution.

I also wanted to observe whether zinc would have an effect on oligomerization of MDM2. However, as can be seen from the migration of the protein from the 0.1 mM zinc preparation (Figures 4.5, 4.6), the protein in the presence of zinc behaves identically as the wild type. The gel filtration profile is also identical as the preparation without zinc (data not shown). The double band at 95 kDa is unchanged and the gel filtration profile still shows the previously described heterogeneous oligomeric peak (data not shown). I can conclude that MDM2 oligomerization is heavily mediated by contacts other than the zinc coordinating domains. Another unexplored variable would be to increase the concentration of zinc in the protein preparations, as the concentration of zinc could be a factor.

MDM2 Δ C7 exhibits wild type behavior in gel filtration column

The deletion of the last 5-7 amino acids of the RING domain in MDM2 Δ C5 (400-486) and MDM2 Δ C7 (400-484) seems to abolish the supramolecular assembly of the RING domain as monomers were observed in gel filtration (Poyurovsky *et al*). However, the MDM2 Δ C7 (1-484) construct is less drastically modified as it is based on the full length protein, and shows the same broad oligomerized peak in gel filtration as the wild type protein (Figure 4.9)

The truncation protein also exhibits an unseen behavior of hindered migration in a 10% SDS-PAGE (Figure 4.7). This suggests that the charge

properties of the protein are altered after the removal of the highly hydrophobic side chains (M,I,V,L,T,Y,F). We hypothesized from the results of Poyurovsky *et al.* that the supramolecular assembly of the RING domain mediated by the hydrophobic interactions would be disrupted in our construct MDM2 Δ C7 (1-484). However, the large difference between my construct (1-484) and the construct in Poyurovsky's study (400-484) suggests that MDM2 oligomerization is mediated not only by the hydrophobic RING domain, but also by other domains of the protein.

We also investigated whether the presence of 0.1 mM zinc chloride would have an effect on the oligomerization of the truncated mutant. However, 10% SDS-PAGE and western blot show that the protein behaves the same with and without zinc (Figure 4.8). Also in the gel filtration chromatogram of the truncation mutant with zinc, no monomer peak appeared and the chromatographic profile resembled that of the oligomerized wild type MDM2. The truncation mutant results suggest that the hydrophobic residues of the RING domain as well as the interactions of cysteines do not exclusively explain the MDM2 oligomerization.

However, when I ran the truncated mutant of both non-zinc and zinc preparations in a 7% SDS-PAGE, both proteins entered the gel and ran as a single band of 95 kDa (Figure 4.10). A single band for a MDM2 preparation is a previously unseen behavior and it suggests that deleting the last seven amino acids of the RING domain does have an effect on altering the heterogeneity that normally produces the double band. The single-band effect in SDS-PAGE,

however, is only distinguishable under heat and reducing conditions, but not in gel filtration experiments. We still cannot explain the abnormally slow migration of MDM2 in SDS-PAGE (expected 56 kDa vs. experimental 95 kDa), but we can assume that the 95 kDa species is a 112 kDa MDM2 dimer that runs lower than predicted due to MDM2's acidic charges ($pI=4.72$). From this analysis, I came to the conclusion that 0.1 mM $ZnCl_2$ is not a high enough concentration to produce any notable effect in the mutant.

MDM2-MBP exhibits oligomerization

Western blots of anti-his and anti-MBP antibodies show a MDM2-MBP migration at 130 kDa in 10% SDS-PAGE (Figures 4.11). In gel filtration chromatography, MDM2-MBP eluted as the broad middle peak (Figures 4.12, 4.13). The pure fraction was concentrated and studied with the electron microscope. Figure 4.14 shows uniform circular bodies visible in white that are thought to be a homogenous sample of MDM2-MBP. These micrographs were compared with class averages of the wild type MDM2 obtained previously in our lab (Figure 4.15). These class averages show different sizes of the particle indicating different oligomerization states of the wild type MDM2. However, the MDM2-MBP micrographs differ by showing a uniform circular species. This indicates that the oligomerization of MDM2 was prevented by the bulky MBP tag on the C terminus of MDM2 where oligomerization is mediated by the C-terminal RING domain.

Presence of p53CT alters MDM2 oligomerization

The His-MDM2/MBP-p53CT complex purification with the his-tag showed a novel single band of MDM2 between 43-55 kDa on a western blot with anti-his antibody (Figure 4.16). However with anti-MBP antibody, no MBP-p53CT was detected. This suggests that although MBP-p53CT has been washed away from the column during purification, its presence during expression has altered the MDM2 oligomerization. A single band between 43-55 kDa shows that it is a monomer of MDM2, running below its theoretical molecular weight of 56 kDa due to the negative charge of the protein. In the MBP tag purification, the same observation is made for the MDM2 migration (data not shown). The presence of MBP-p53CT seems to interfere with MDM2 oligomerization, which is in agreement with the literature observations that p53CT interacts with MDM2 N- and C-termini.

Discussion

Through our experiments, we were able to observe different behaviors of MDM2 in SDS-PAGE and in gel filtration. This observation suggests that protein oligomerization was altered.

In our MDM2 Δ C7 mutant, we observed the same gel filtration behavior as the wild type showing the predominant oligomer peak around 669kDa. This indicates that the oligomerization of the full length protein is mediated not only by

the last seven residues of MDM2 but by other parts of the protein as well. The presence of 0.1mM Zn^{2+} did not appear to have an effect on MDM2 oligomerization. However, deletion of the seven hydrophobic residues altered the protein migration on SDS-PAGE. When observed under a lower percentage gel, a novel banding pattern of a single band appeared as opposed to the double band that was seen previously with the wild type. This suggests that an unknown mediation of MDM2 dimer that produces the double band was altered in the truncation mutant, and this observation is only prevalent under the reducing and heated condition. It is interesting that this effect does not seem to alter the higher-order supramolecular assembly in gel filtration. This enigmatic double band therefore is originated from an interaction through the extreme C-terminus of the RING domain. And from the molecular weight of 95kDa of the band, it can be suggested that the functional unit of MDM2 truncation mutant is a dimer that does not become disrupted even in the reducing and heated conditions.

Our MDM2-MBP mutant was created next to achieve monomers of the protein. We reasoned that a bulky 43kDa MBP tag on the C-terminus near the oligomerization RING domain would interfere with the supramolecular assembly of the protein. As expected, the electron micrographs reveal homogeneous fractions of MDM2-MBP as compared to that of the wild type MDM2, confirming that the bulky MBP tag has prevented the supramolecular assembly of the protein.

Finally, co-expression of 6xHis-MDM2 with MBP-p53CT produced a novel observation of MDM2 monomers in SDS-PAGE gel. This indicates that the interaction of p53CT with MDM2 abolished the MDM2 oligomerization. The next step is to complex the monomers of MDM2 with p53 for elucidation of its structure. This complex structure would help in understanding the structure of the p53 regulatory domain.

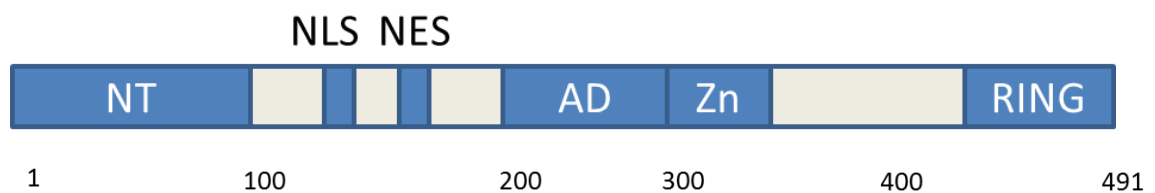


Figure 4.1 Domains of MDM2. MDM2 is composed of four major domains. The N-terminal domain (NT) binds to p53 for inhibition of p53 function. The acidic domain (AD) contacts the p53 DBD to inhibit p53's specific DNA binding activity. Zinc finger domain (Zn) coordinates zinc for stability of folding. The RING domain, which is the oligomerization domain, acts as the E3 ubiquitin ligase in ubiquitinating p53. NLS and NES allow nuclear transport of the protein.

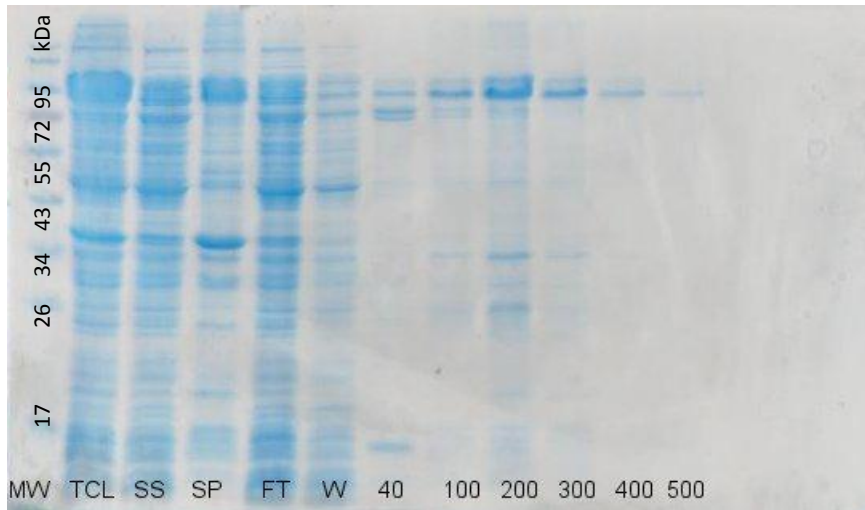


Figure 4.2 SDS-PAGE of 6xHis MDM2 Purification. 10% SDS-PAGE Coomassie gel of a MDM2 preparation. TCL, total cell lysate; SS, spin supernatant; SP, spin pellet; FT, flow through; W, wash with lysis buffer, and 40-500mM Imidazole wash and elutions. MDM2 appears as a double band at around 95kDa.



Figure 4.3 Western Blot of 6xHis MDM2 Purification. 10% SDS-PAGE gel was transferred onto a nitrocellulose paper, and blotted with anti-His antibody. The lanes are analogous to those in Figure 4.2. In 200mM imidazole fraction, degradation of MDM2 can be seen.

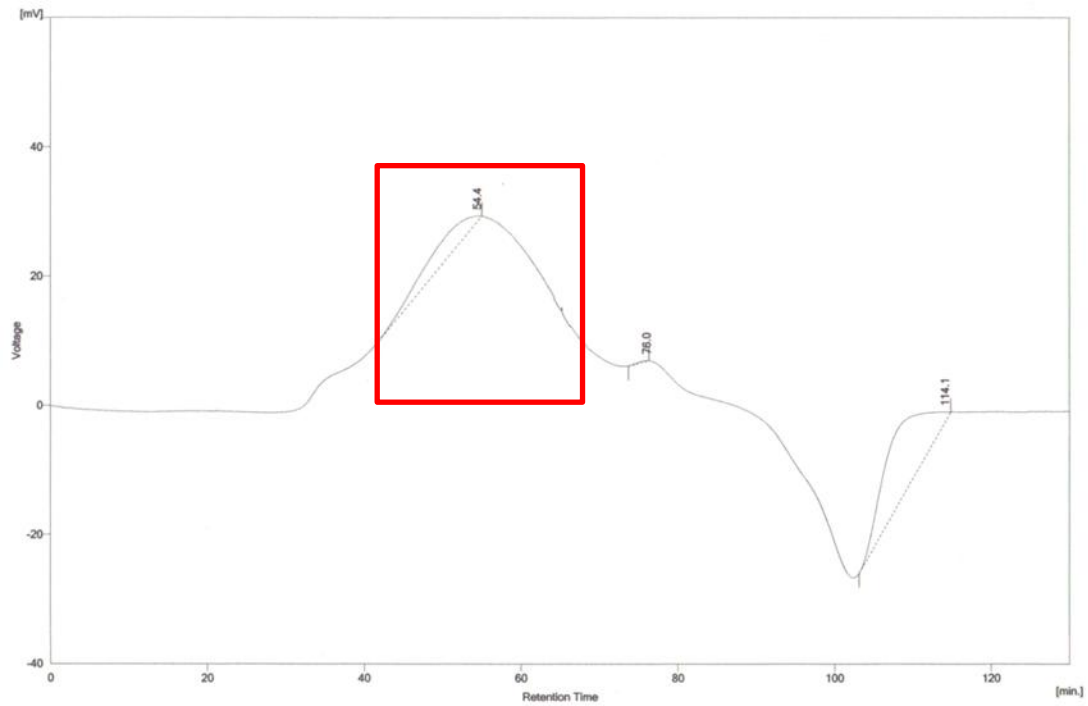


Figure 4.4 Gel filtration chromatogram of wild type MDM2. The wild type MDM2 protein in the absence and in the presence of zinc shows the identical peak around 55 minutes shown on this chromatogram using Superose 6 gel filtration column. The smaller side peaks are also identical in the zinc and non-zinc preparations.

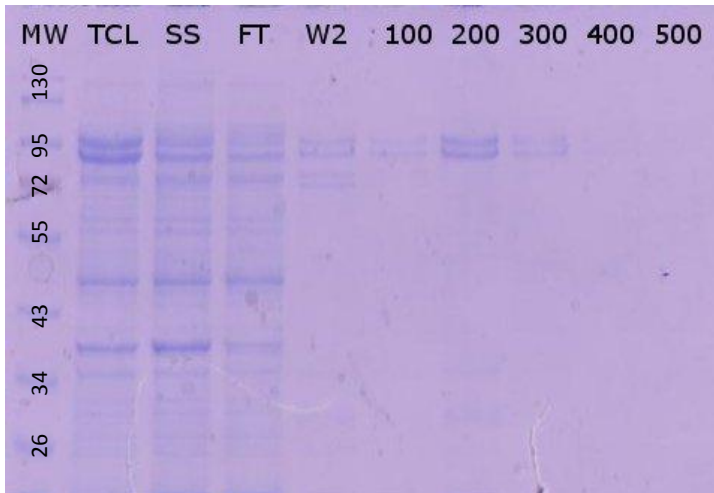


Figure 4.5 10% SDS-PAGE of wild type MDM2 preparation with 0.1 mM zinc chloride. The gel looks identical to that of the non-zinc prep shown in Figure 4.2. The double band pattern at 95kDa is still prevalent.

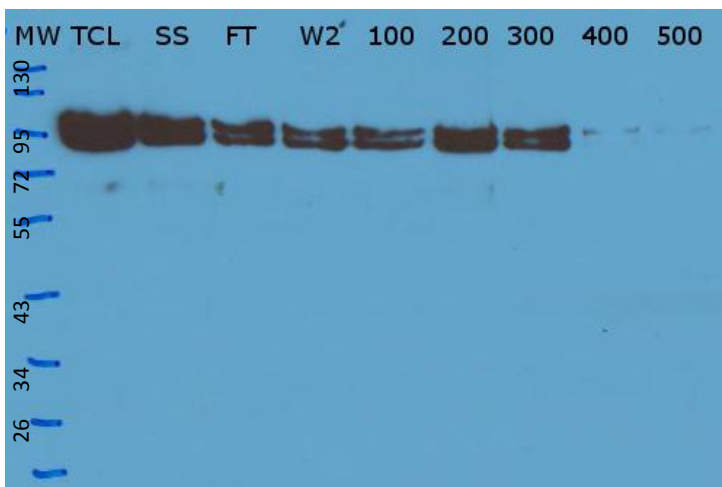


Figure 4.6 Western blot of wild type MDM2 preparation with 0.1mM zinc chloride, blotted with anti-his antibody. The western blot corresponds to the Coomassie gel in Figure 4.5.

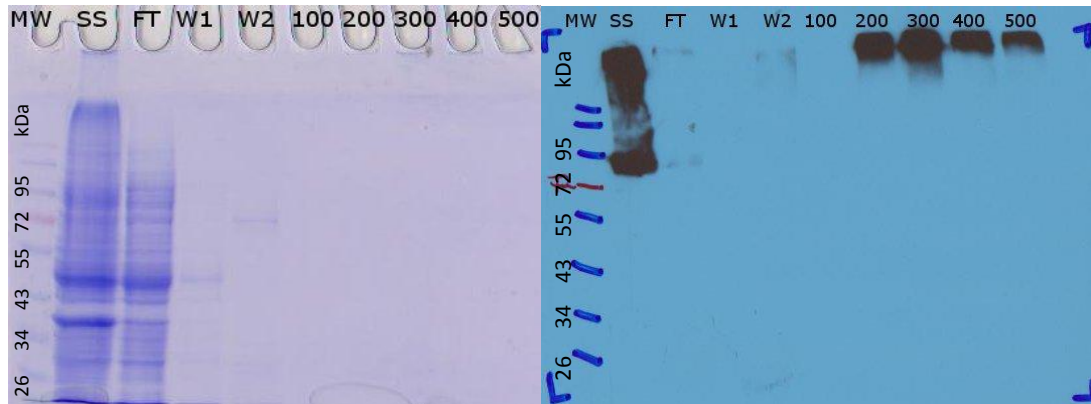


Figure 4.7 Preparation of MDM2 Δ C7 resolved in 10% SDS-PAGE. Truncated mutant was resolved in 10% SDS-PAGE and blotted with anti-his antibody. It reveals that the protein did not enter the gel.

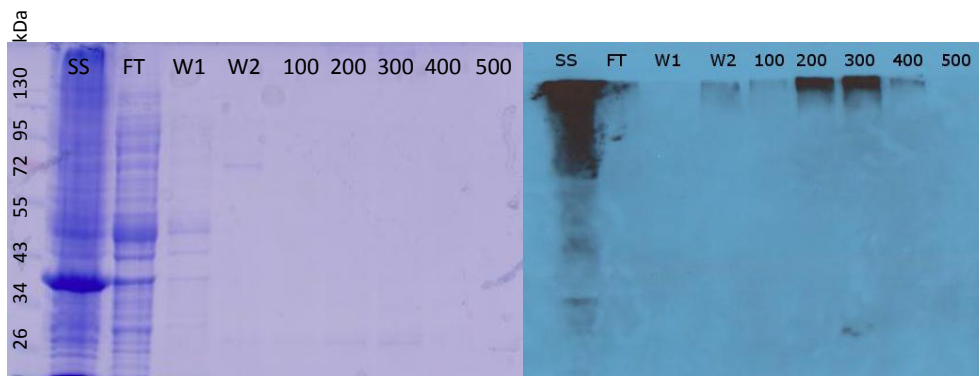


Figure 4.8 Truncated MDM2 Δ C7 mutant with 0.1 mM zinc chloride. Visualized by Coomassie staining and blotted with anti-his antibody on 10% SDS-PAGE. Preparation of the truncation mutant with zinc does not seem to differ from the preparation without zinc shown in Figure 4.7.

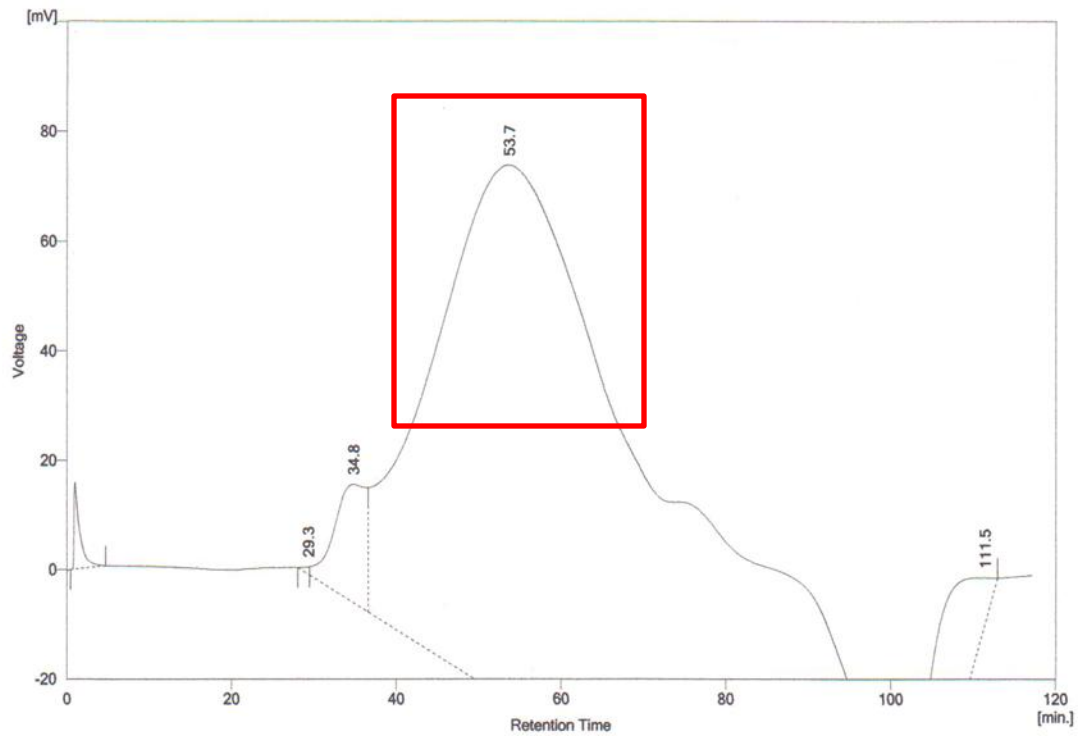


Figure 4.9 Gel filtration profile of the truncated mutant MDM2 Δ C7. For both in the presence or in the absence of 0.1 mM zinc chloride, the gel filtration (Superose 6) profile of the truncated mutant has the oligomerized peak at around 54 minutes. This peak also matches the oligomerized peak for the wild type MDM2 protein shown in Figure 4.4.

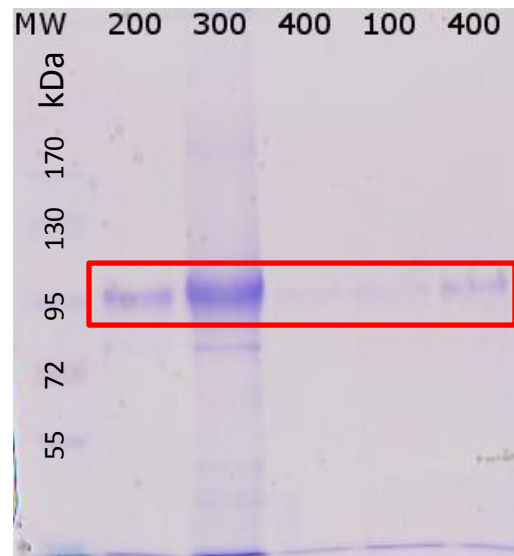


Figure 4.10 Truncated mutant resolved in 7% SDS-PAGE and visualized by Coomassie staining. The first three lanes contain the truncated mutant from the non-zinc preparation. The last two lanes contain the truncated mutant from the zinc preparations. For both preparations, when resolved in a lower percentage 7% SDS-PAGE, the protein migrates as a single band at 95kDa.

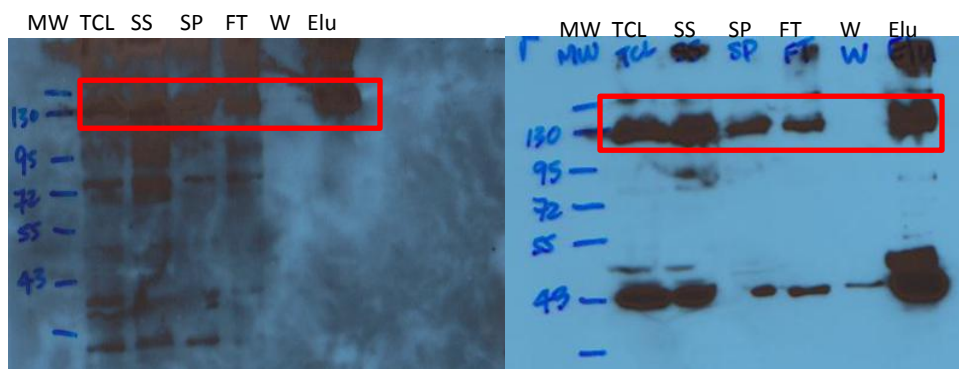


Figure 4.11 Western blots of MDM2-MBP Preparation. The 130kDa band was confirmed as the MDM2-MBP fusion protein in the preparation blotted with both anti-his (left) and anti-MBP (right) antibodies.

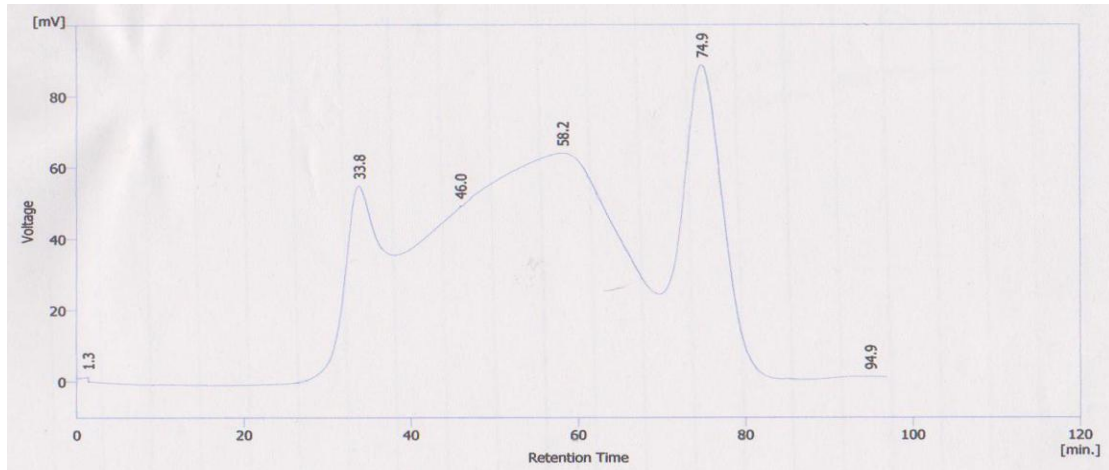


Figure 4.12 Gel filtration profile of MDM2-MBP. Superpose 6 gel filtration column revealed three peaks for MDM2-MBP sample.

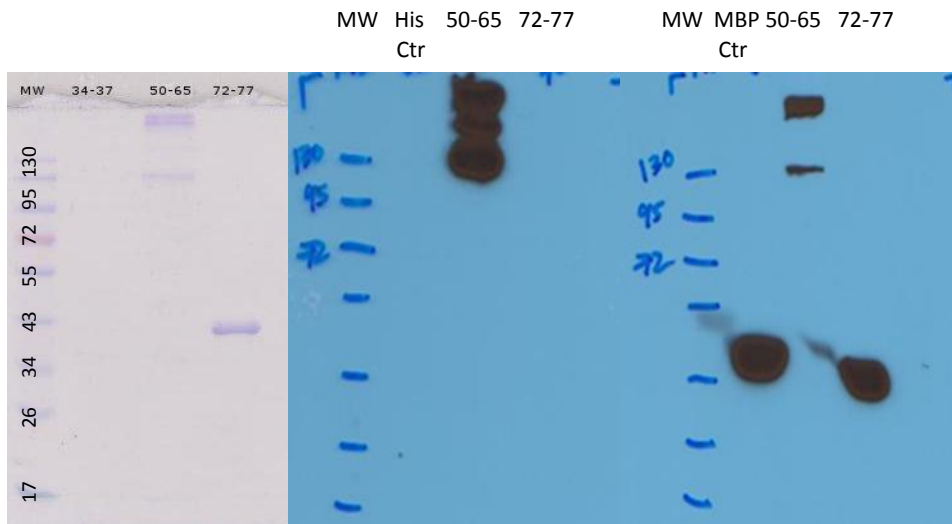


Figure 4.13 Fractions of MDM2-MBP gel filtration profile concentrated and resolved in 10% SDS-PAGE. Visualized by Coomassie staining (left), and blotted with anti-his antibody (middle), and with anti-MBP antibody (right). It is revealed that the middle peak from Figure 4.12 contains the desired MDM2-MBP.

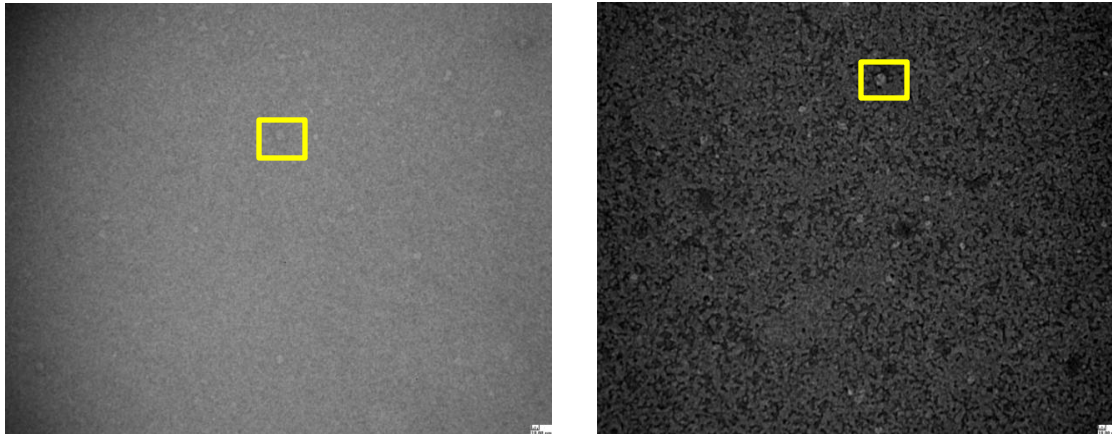


Figure 4.14 Electron micrographs of MDM2-MBP. Negative stained electron micrographs show MDM2-MBP as the circular particles boxed in yellow. They exist in a homogeneous fraction.

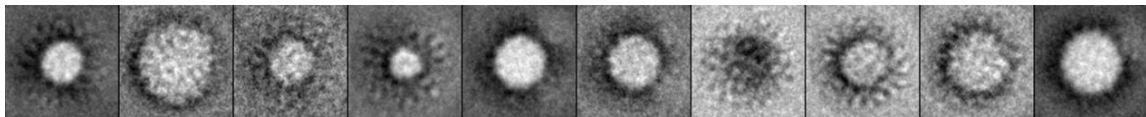


Figure 4.15 Electron micrographs of wild type MDM2. Class averages of MDM2 wild type proteins show particles existing in heterogeneous fashion where the sizes of each particle differ from one another. This indicates the existence of different oligomers of MDM2.

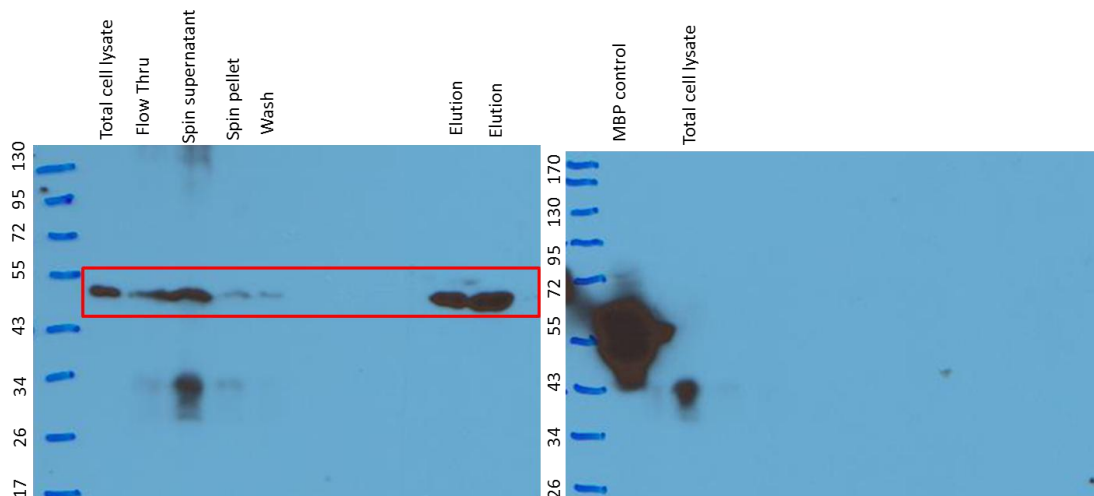


Figure 4.16 Co-expression experiment of MDM2 and p53CT. Blotted with anti-his antibody (left), and with anti-MBP antibody (right). A novel band just below the 55kDa mark was observed in the anti-his blotted western. This band suggests that the monomers of MDM2 are present in the presence of p53CT.

References

- Clegg, H. V.; Itahana, K.; Zhang, Y., Unlocking the Mdm2-p53 loop: ubiquitin is the key. *Cell Cycle* **2008**, 7 (3), 287-92.
- Cross, B.; Chen, L.; Cheng, Q.; Li, B.; Yuan, Z. M.; Chen, J., Inhibition of p53 DNA binding function by the MDM2 protein acidic domain. *The Journal of biological chemistry* **2011**, 286 (18), 16018-29.
- Freedman, D. A.; Wu, L.; Levine, A. J., Functions of the MDM2 oncoprotein. *Cellular and molecular life sciences : CMLS* **1999**, 55 (1), 96-107.
- Kawai, H.; Lopez-Pajares, V.; Kim, M. M.; Wiederschain, D.; Yuan, Z. M., RING domain-mediated interaction is a requirement for MDM2's E3 ligase activity. *Cancer research* **2007**, 67 (13), 6026-30.
- Kussie, P. H.; Gorina, S.; Marechal, V.; Elenbaas, B.; Moreau, J.; Levine, A. J.; Pavletich, N. P., Structure of the MDM2 oncoprotein bound to the p53 tumor suppressor transactivation domain. *Science* **1996**, 274 (5289), 948-53.
- Lane, D. P.; Cheok, C. F.; Brown, C.; Madhumalar, A.; Ghadessy, F. J.; Verma, C., Mdm2 and p53 are highly conserved from placozoans to man. *Cell Cycle* **2010**, 9 (3), 540-7.
- Lindstrom, M. S.; Jin, A.; Deisenroth, C.; White Wolf, G.; Zhang, Y., Cancer-associated mutations in the MDM2 zinc finger domain disrupt ribosomal protein interaction and attenuate MDM2-induced p53 degradation. *Molecular and cellular biology* **2007**, 27 (3), 1056-68.
- Ma, J.; Martin, J. D.; Zhang, H.; Auger, K. R.; Ho, T. F.; Kirkpatrick, R. B.; Grooms, M. H.; Johanson, K. O.; Tummino, P. J.; Copeland, R. A.; Lai, Z., A second p53 binding site in the central domain of Mdm2 is essential for p53 ubiquitination. *Biochemistry* **2006**, 45 (30), 9238-45.
- Maki, C. G., Oligomerization is required for p53 to be efficiently ubiquitinated by MDM2. *The Journal of biological chemistry* **1999**, 274 (23), 16531-5.
- Michael, D.; Oren, M., The p53-Mdm2 module and the ubiquitin system. *Seminars in cancer biology* **2003**, 13 (1), 49-58.
- Nicholson, J.; Hupp, T. R., The molecular dynamics of MDM2. *Cell Cycle* **2010**, 9 (10), 1878-81.

Popowicz, G. M.; Czarna, A.; Rothweiler, U.; Szwagierczak, A.; Krajewski, M.; Weber, L.; Holak, T. A., Molecular basis for the inhibition of p53 by Mdmx. *Cell Cycle* **2007**, 6 (19), 2386-92.

Poyurovsky, M. V.; Priest, C.; Kentsis, A.; Borden, K. L.; Pan, Z. Q.; Pavletich, N.; Prives, C., The Mdm2 RING domain C-terminus is required for supramolecular assembly and ubiquitin ligase activity. *The EMBO journal* **2007**, 26 (1), 90-101.

Poyurovsky, M. V.; Katz, C.; Laptenko, O.; Beckerman, R.; Lokshin, M.; Ahn, J.; Byeon, I. J.; Gabizon, R.; Mattia, M.; Zupnick, A.; Brown, L. M.; Friedler, A.; Prives, C., The C terminus of p53 binds the N-terminal domain of MDM2. *Nature structural & molecular biology* **2010**, 17 (8), 982-9.

Schon, O.; Friedler, A.; Freund, S.; Fersht, A. R., Binding of p53-derived ligands to MDM2 induces a variety of long range conformational changes. *Journal of molecular biology* **2004**, 336 (1), 197-202.

Shloush, J.; Vlassov, J. E.; Engson, I.; Duan, S.; Saridakis, V.; Dhe-Paganon, S.; Raught, B.; Sheng, Y.; Arrowsmith, C. H., Structural and functional comparison of the RING domains of two p53 E3 ligases, Mdm2 and Pirh2. *The Journal of biological chemistry* **2011**, 286 (6), 4796-808.

Teufel, D. P.; Bycroft, M.; Fersht, A. R., Regulation by phosphorylation of the relative affinities of the N-terminal transactivation domains of p53 for p300 domains and Mdm2. *Oncogene* **2009**, 28 (20), 2112-8.

Uldrijan, S.; Pannekoek, W. J.; Vousden, K. H., An essential function of the extreme C-terminus of MDM2 can be provided by MDMX. *The EMBO journal* **2007**, 26 (1), 102-12.

Wade, M.; Wahl, G. M., Targeting Mdm2 and Mdmx in cancer therapy: better living through medicinal chemistry? *Molecular cancer research : MCR* **2009**, 7 (1), 1-11.

Wallace, M.; Worrall, E.; Pettersson, S.; Hupp, T. R.; Ball, K. L., Dual-site regulation of MDM2 E3-ubiquitin ligase activity. *Molecular cell* **2006**, 23 (2), 251-63.